Master's Thesis

Molecular Dynamics Simulation of Copper Deposition by Ion Beam Assisted Deposition and Physical Vapour Deposition Technique

Alex Odiyo

Supervisor: Antti Kuronen, PhD
Examiners: Antti Kuronen and Professor Kai Nordlund

HELSINGIN YLIOPISTO
HELSINGFORS UNIVERSITET
UNIVERSITY OF HELSINKI

MATEMAATTIS-LUONNONTIETEELLINEN TIEDEKUNTA
MATEMATISK-NATURVETENSKAPLIGA FAKULTETEN
FACULTY OF SCIENCE

Tiedekunta – Fakultet – Faculty		Koulutusohjelma – Utbildningsprogram – Degree programme
Science		Degree Programme in Physical Sciences
Tekijä – Författare – Author		
Alex Nyakumba Odiyo		
Työn nimi – Arbetets titel – Title		
Molecular Dynamics Simulation of Copper Deposition by Ion Beam Assisted Deposition and Physical Vapour Deposition Technique		
Työn laji – Arbetets art – Level	Aika – Datum – Month and year	Sivumäärä – Sidoantal – Number of pages
Master's	June 2019	57

Tiivistelmä – Referat – Abstract

Physical Vapour Deposition (PVD) is a method of thin film deposition that involves transport of materials in the gas phase through physical means. The greatest advantage of using PVD is its ability to deposit hard coatings that are almost impossible to deposit by other liquid or chemical deposition methods. The applications of PVD include semiconductor devices, cutting and drilling tools, optical coating for displays, and decorative coatings for jewellery. When PVD process is accompanied by a separate (noble) gas ion bombardment, it is termed as Ion Beam Assisted Deposition (IBAD). These two processes can be subjected to atomistic simulation as opposed to conventional experimental methods. The idea behind such a simulation is the level of control in terms of material purity, dimensionality and simulation parameters.

In this simulation work, the growth and overall morphology of epitaxial growth of copper film under both PVD and IBAD is considered. The film roughness and intrinsic stress are subjected to testing under various deposition energies in PVD. The same properties are also tested under variation of bombardment energies, and bombarding rates or ion fluence in IBAD.

The results show that the nature of the film growth is primarily dependent on the deposition energy. In PVD, low deposition energies lead to growth dominated by island growth, while high deposition energies are mainly layer-by-layer growth dominated. In IBAD done at a constant low atom deposition energy, a similar trend is seen with an increasing argon ion bombardment energy at 0.5 ions/nm^2 fluence. Since the deposition energy of 1 eV is geared towards island growth, the conversion rate of island like structures to relatively layer-by-layer structure depends on the ion bombardment energy (IBAD case).

By comparison of IBAD and PVD outcomes, it has been established that the best layered PVD film occurs at a deposition energy of 30 eV. The overall film quality (in PVD) with respect to layer-by-layer growth is much better than that deposited using IBAD at similar bombardment energy at an ion fluence 0.5 ions/nm^2. However, to attain a comparable or superior layer-by-layer growth as PVD, IBAD process has to be conducted at a much higher bombardment energy (50 eV) at fluence of 0.5 ions/nm^2. The other alternative is to undertake IBAD process at bombardment energy of 30 eV, and at a much higher ion fluence. At a fluence of 0.8 ions/nm^2 and equivalent ion bombardment energy (30 eV) produces a far much superior structure to PVD growth. The tradeoff between which ion fluence to use in IBAD is the deposition rate. Higher ion fluence translates to slow deposition but much improved layer-by-layer structure.

The stress profile shows a decreasing stress profile as a function of thickness as predicted by Stoney's equation. At non-equilibrium deposition conditions, the film is generally stressed. However, under optimal conditions for layer-by-layer growth, IBAD grown films are generally less stressed in comparison to PVD.

Avainsanat – Nyckelord – Keywords
Physical Vapour Deposition (PVD) , IBAD, growth modes, Molecular Dynamics (MD) simulation, Surface roughness, Surface stress

Säilytyspaikka – Förvaringställe – Where deposited
HELDA - Digital Repository of the University of Helsinki

Muita tietoja – Övriga uppgifter – Additional information

Contents

Abstract i

Introduction 1

1 Physical Vapour Deposition 3
- 1.1 Surfaces and Interfaces . . . 3
- 1.2 Films and Substrates . . . 6
- 1.3 Physical Vapour Deposition Technique . . . 7
- 1.4 Film Uniformity and Conformality . . . 8
- 1.5 Ion Beam Assisted Deposition . . . 10
- 1.6 Growth Modes . . . 11
  - 1.6.1 Thermodynamic model . . . 12
  - 1.6.2 Atomic model . . . 14
- 1.7 Columnar and Grain Growth . . . 14
- 1.8 Energetic Particles . . . 17
- 1.9 Applications of PVD . . . 18
- 1.10 Modeling PVD . . . 19

2 Molecular simulations 22
- 2.1 Introduction . . . 22
- 2.2 Simulation scale . . . 24
- 2.3 Simulation and Ensemble Averages . . . 25
- 2.4 Interactions and Potentials . . . 26
  - 2.4.1 Embedded Atom Method . . . 27
  - 2.4.2 Ziegler-Biersack-Littmark potential . . . 28
- 2.5 Boundaries . . . 29
- 2.6 Temperature Control . . . 30
- 2.7 Integrators . . . 31
- 2.8 Molecular Dynamics Simulation Algorithm . . . 32
- 2.9 Growth simulations in MD . . . 33
- 2.10 Thesis simulations . . . 34
- 2.11 Surface roughness and stress analysis . . . 36

3 Results 38
- 3.1 Effect of energy on layer growth . . . 41
- 3.2 Effect of Ar ion fluence on layer growth . . . 44
- 3.3 Film Stress . . . 46

Conclusion 50

References 51

Introduction

Over the years, most electronic devices have been made smaller or retained their size but obtained increased functionality. This progress in device fabrication is a result of circuit miniaturization, 3D multi-packaging and advanced integration [1,2]. The actual trend was predicted by Moore in 1965 - the so famously coined Moore's law [2]. This process has made headway as a consequence of necessity and unwavering contributions from multiple scientists despite multiple criticisms and enormous challenges encountered [2]. Currently, research has reached a point at which materials can be confined in three dimensions (artificial atoms) [3]. In this thesis, the scope will be limited to materials that are confined in a single spatial dimension, commonly termed as thin films. Thin films are also called coatings or depositions in other disciplines [4].

The current available technology has facilitated the controlled growth of thin films that have found applications in high-end optical equipment, magnetic articulated equipment and semiconductor device fabrication. This is made possible through exploitation of the material properties at the very fundamental level i.e. atomic and molecular levels [1,3,4]. This level of exploit, in a more or less general approach, borders on two crucial approaches. There is an experimental approach that produces final product and computer modelling (or simulation) processes that aid in handling intermediary and trial processes. These two combinations ensure amongst others, exploitation of superior growth and material characterization techniques, means of estimating growth parameters and minimization of waste from a growth processes [5,6].

Device fabrication consists of multiple steps inclusive of selection and treatment substrates, deposition, lithography, etching, integration and a repeat of either the aforementioned processes. At times bonding and dicing as well as ion implantation and thermal annealing may be incorporated in the process [1,3,4]. However, for the purpose of this thesis, the scope is restricted to deposition process. Even with this limitation, there are many technicalities such as film stress control, structural and topographical predictability amongst others that arise in a deposition process [4,9]. Therefore, thin films deposition is not a form of light laboratory excursion but a serious scientific process that requires a lot of theoretical background and extensive knowledge of materials.

Physical vapour deposition (PVD) is a potential ubiquitous deposition technique. It has been implemented in optical equipment production, electronic device fabrication and as an industrial scale coating of metals for protection against multiple forms of wear. This method uses a direct evaporation process followed by condensation on a substrate and hence can be used deposition very hard and stable chemical elements or compounds such as TiN, CrC and CrN [7]. This method can be implemented alongside an independent bombardment source. This transitions PVD to ion beam assisted deposition (IBAD). IBAD improves PVD by favouring growth of densely packed films. This is because, at optimal bombardment energies, the bombardment cycle eliminates potential vacancies and voids, and allows for heterogeneous nucleation [9].

Deposition methods are not exclusive to PVD and IBAD. There exist many other gas and liquid phase methods inclusive of electroplating, atomic layer deposition(ALD) and chemical vapour and solution deposition (CVD & CSD). Despite the method of deposition adopted, the underpinning scientific guidelines will still apply. One of the aspects is that every thin film deposition process through an experiment or a simulation is conducted in a way that it is reproducible. In addition, a deposition process should be controllable such that the desired properties of the film are met (deposition objective) [4,8]. To achieve an experimental objective, measurement methods must be incorporated in the deposition process. These methods are used to measure quantitatively and qualitatively the film during deposition and after deposition. These methods are collectively called (thin film) characterization techniques and include radiation and electronic based measurement techniques amongst others [4,11]. From a simulation point of view, measurements are done through statistical analysis which are then correlated to corresponding material properties.

To understand the dynamics of thin film deposition, information on the nature of surfaces is necessary. This is because surfaces influence adhesion properties of an adsorbent, quality and properties of film (or multi-film) structure amongst others [4]. Knowledge of surface composition and morphology influences the nature and extent of surface treatment before a deposition process. The importance of surface details increases with the sensitivity of the projected outcome. For example, a lot of surface details and precision is needed in handling materials for making integrated circuits.

Information on the growth processes may not be the end. Many other materials may need to be incorporated within the pre-existing film. It is necessary to have a platform to experiment on (or extrapolate results to) other available material or material combinations. For the purpose of prototyping, only the initial results matter most. However, for mass production deposition cases, process efficiency has to be maximized. To attain such ambitious objectives, a virtual laboratory is needed in place of a physical laboratory. This is made possible by computer simulations. The actual physical processes are mimicked through a computer program. In the program, the various material properties, experimental conditions etc. are represented as variables or parameters. Then, as many as possible variable combinations can be tested and visualized [5, 11].

Computer simulation processes have improved in efficiency courtesy of high-end technological and computational advancements. This has translated to greater capacity and range of implementation of simulations. Simulations are now being used in large scale studies of physical phenomena with an interest of understanding fundamental mechanisms behind those processes. For example, through simulations, many atomic processes that are very fast to the extent of taking place unnoticed during a deposition process can be observed or analysed. This is because a simulation system can be slowed down or be frozen at any instance. Such a capability provides an opportunity to reveal hidden insights or mechanisms in a deposition processes [5]. Moreover, on the front of scarce materials and unknown materials, simulations may provide insights to material dynamics or shape expectation of outcome.

Simulating thin film deposition process requires complex algorithms. At times, due to the complexity, isolated algorithms that describe or analyze the various parts of the deposition process are aggregated. In other cases, the same deposition process with different set of materials may demand for adjusted or new algorithm to describe the process [6]. Despite all these, the fundamental consideration in applying simulations to deposition processes is to be able to investigate the fundamental limits of test materials under certain conditions. Secondly, is to observe the effect of simulation variables i.e. response of the deposition process to variation of simulation variables. Thirdly, is to optimize already known process with an expectation of improving the deposition process. Lastly, to stretch the limits of imagination i.e. expand the optimized results to different range of possible candidate materials [5, 6].

The simple modification of virtual components and theirn superior control makes computer simulations sounds like a soft hymn in comparison to experimental counterparts. This is not the case. A model is required in order for simulation to be done. The development of a suitable model from a theoretical or experimental framework is not trivial. A wrong model will result in bad results. The contretemps of using simulations is that - no matter the level of designing and execution expertise - it requires an experimental validation mechanism. This is because the maxim of science is always tilted in favour of experimental results. This, however, does not diminish the potential of simulations.

1 Physical Vapour Deposition

1.1 Surfaces and Interfaces

A solid surface is the outermost layer or top boundary of material consisting of atoms that separate the solid from the vacuum or atmosphere. In the event that there is discontinuity in the continuous atomic layer within the surface, then, it is termed an interface [14]. However, the definition of interface is much broader in the sense that even a solid surface is a kind of special interface. Surfaces have their inherent properties, such as heterogeneity and texture, that may be totally different from bulk properties [20]. Many, but not all, deposition processes are done on surfaces or the sub-surface. This makes the fundamental understanding of the nature surfaces extremely crucial. For example, poor consideration of surface properties may lead to cracking of film, formation of semi-crystalline instead of crystalline interface amongst other surface artefacts [4].

To have basic understanding of the nature of surfaces, a hypothetical surface is formed by splitting bulk (crystalline) material. It is observed that the surface atoms have unsaturated bonds (also called dangling bonds) which leads to an imbalance of surface electronic structure. This imbalance is compensated through a number of processes inclusive of formation of surface defects, surface relaxation (in metals), surface reconstruction, or adsorption of some atmospheric gases such as oxygen and hydrogen [14, 15, 19–22]. The driving mechanisms for some of these processes are hidden in complex morphology physics, reaction and coordination chemistry at cleavage. The actual final adopted surface structure is a contribution of both surface stress σ and specific surface free energy γ.

At the point of splitting a bulk material, two surfaces are obtained. Assuming that the material is homogeneous and of good distribution (devoid of huge voids), then, consideration of only one surface is sufficient for analysis. The newly created surface attempts to modulate the effects of the changes in the forces resulting from the alteration of charge distribution. This transformation results in some form of stress σ at the surface that propagates in decaying fashion inwards to the bulk layers i.e. the stress is maximum at the surface and diminishes along the direction perpendicular to the surface (say along z axis) [14]. Expressing this stress explicitly in its tensor form as $\sigma = \sigma_{ij}$, the variation of stress can be expressed as:

$$\sigma_{ij}^{s} = \int_{-\infty}^{0} dz \left[\sigma_{ij}(z) - \sigma_{ij}^{b}\right] \tag{1}$$

Here, the indices i and j depict the lateral components of the stress tensor. The superscript s and b are for surface and bulk representation.

Splitting of the bulk material can be done through cleavage or through straining the solid. Either way, the net outcome is that the neighbouring atomic bonds along the separation point are broken and exposed to the vacuum. To narrow down the analysis, I will enforce that the newly formed surfaces are as a result of straining a bulk solid material. This process costs energy. This energy can be represented as work done (δW) in surface creation:

$$\delta W = 2A \sum_{ij} \sigma_{ij} \delta\varepsilon_{ij} \tag{2}$$

Here $\delta\varepsilon_{ij}$ is the strain tensor associated with straining of the bulk material, A is the surface area, and the factor 2 accounts for two surfaces that are formed during the split. This definition of work is limited to the surface, and contribution from the bulk is excluded.

The driving force that initiates surface processes is not only the stress but also the surface free energy. In the limit of constant temperature and number of particles, the work done in creating the surface is equal to the surface free energy F i.e. $\delta W = \delta F$ [14]. By definition, $F = \gamma A$, where γ is the specific surface free energy and A is surface area. Using this newly defined relation between work done and free energy, γ is defined as the reversible work in the formation of unit area under the constraint of fixed system's volume, constant temperature and chemical potential.

The free energy F changes when the number of surface atoms changes at fixed average area per surface atom, this is the case γdA. Modification of surface energetics (e.g. changes in interatomic distances) at constant number of atoms also affects F. This is the second case ($Ad\gamma$). These two case can illustrated as follows:

$$dF = d(\gamma A) = \gamma dA + Ad\gamma \tag{3}$$

Observing the condition of fixed number of particles, combining Equation 2 and 3, the Shuttleworth Equation 4 relating strain, stress and specific surface free energy can be derived. In this equation, the first term of Equation 3 has been dropped for violation of constant particle number and the explicit definition of $dA = A\sum_{ii}\varepsilon_{ii}$ has been used.

$$\sigma^s_{ij} = \gamma\delta_{ij} + \frac{\delta\gamma}{\delta\varepsilon_{ij}} \tag{4}$$

The thermodynamic driving force for the optimal atomic arrangement is the direct contribution of the surface stress and surface free energy. This is can be deduced by rearranging the above equation. Thus, $(\sigma^s - \gamma)$ is the driving force. For some fixed volume, when $(\sigma^s - \gamma) > 0$ translates to a surface attracting more atoms than the bulk while the opposite interpretation holds for $(\sigma^s - \gamma) < 0$ [14]. These two extreme cases tend to explain the deviation of surface structure from the bulk material.

Surface relaxation occurs when inter-planar spacing of the surface layers changes. This phenomenon is more common in metals where bonding is less redirected and there is a strong delocalization of the electron gas. Assuming that the material is crystalline, these phenomena can be observed by comparing interatomic spacing of the bulk against the spacing between the first three topmost surface layers. The comparison is done along the perpendicular direction to the surface. It is observed that the interatomic spacing of top most layer will be contracted relative to bulk spacing because of the inward charge shift of ionic centers at the surface. This motion is a direct consequence of relaxation of the electronic charge density parallel to the surface. In a more vivid description, surface atoms with lower electronic density tend to be easily attracted to the direction of maximum density. This results in back-bonding of surface atoms to the underneath layers [14, 15], which appears as contraction of the top surface layer towards the bulk.

Surface reconstruction involves change in symmetry or periodicity of surface structure for the case of crystalline solids. This usually happens to annihilate dangling bonds in a material and is most pronounced in semiconductors (e.g. silicon) due to high directional bonds. In metals, this process happens because of lowered energy of electronic bands as opposed to the surface healing experience in many semiconductors [14, 15]. Reconstruction changes the final surface profile and hence the bonding probability of an adatom at a surface site.

In every newly formed surface, some form of either surface dislocations or defects such as kinks, steps, ledges, vacancies and adatoms, as shown in Figure 1, are always present [20–23]. These surface structures or deformities are formed for entropical reasons and at times intrinsic reasons such as crystallographic orientation [14]. For example, in metals, terraces represent areas for which a surface is formed in the vicinity of a low index plane. In the deposition and film growth processes, defects influence the film morphology. For instance, they present areas with unique coordination, binding energies and electronic states [14]. These clean surface abnormalities translate to reactive sites, atom traps, nucleation sites etc.

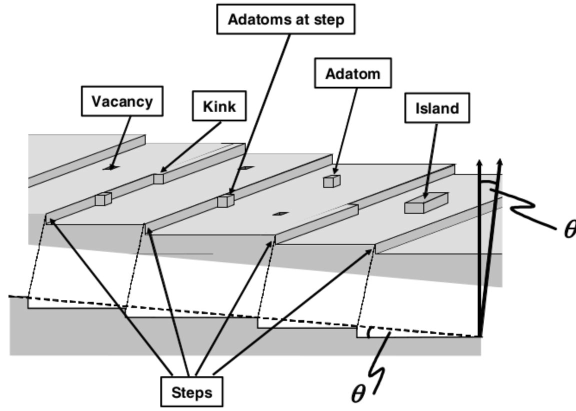

Figure 1: Defects on real surfaces [23]

Surface profiling involves the analysis of the nature of the local variation of local density of steps on that surface. This profile is not always static but may decay or evolve during or after deposition processes. The primary driver for such surface metamorphosis is diffusion. Diffusion plays an active role in transportation of an atom (or mass of atoms) across a surface [14, 15]. However, for surface diffusion to occur, some form of activation energy is needed. To visualize the necessity of activation energy, a clean surface is represented as an array of shallow potential wells as shown in Figure 2a [14]. At any instance, an adatom can be trapped in any of such well. For that trapped atom to navigate or migrate from one potential confinement to another (surface motion or diffusion), a certain amount of energy (activation energy) has to be obtained by the bound atom.

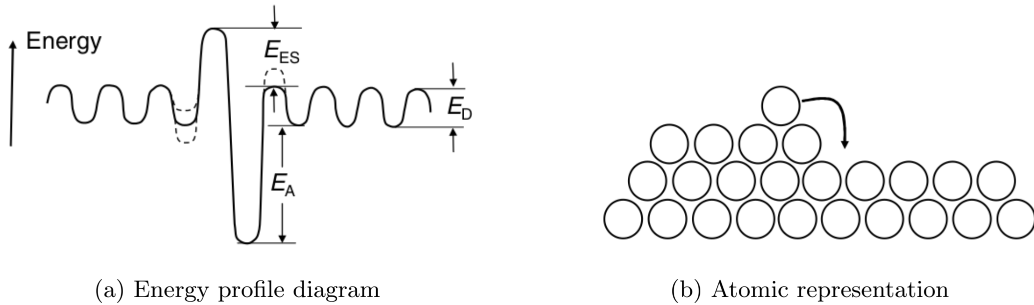

(a) Energy profile diagram

(b) Atomic representation

Figure 2: Surface potential landscape [15]

The set of three energies E_A, E_{ES} and E_D represented on the Figure 2 are the binding energy to a step site, the Ehrlich-Schwoebel barrier, and the activation energy for terrace, respectively. These energies constitute the minimal set of energies required do describe a surface decay profile.

To extend the idea of confinement traps on the surfaces, surfaces that are vicinal to low index orientations are included. This is because such surfaces have both terraces and monatomic steps. The activation energy for interlayer diffusion (over step edge) and intralayer diffusion (across a terrace) are different. This difference in that energy is called step-edge barrier or Ehrlich-Schwoebel barrier (ES-barrier) [15]. The ES-barrier is a direct consequence of the difference in second coordination number of an adatom located on a terrace and the upper side of the step-edge. Therefore, the effective binding energy of the upper step-edge is lower than on a terrace. Alternatively, the atom embedding energy at the upper step-edge is lower than on terrace because of the lower electron density. The higher binding energy at the lower side of the edge -step is due to the larger number of (total first and second) nearest neighbours [14].

1.2 Films and Substrates

In a deposition process, a substrate is defined as the surface on which a thin film is deposited. It can also be defined as a solid surface that acts as a support for a thin film. Substrates usually undergo treatment (cleaned, conditioned, activated etc.) prior to the deposition process in order to have to some level of predictability of surface properties or deposition outcome. However, even known substrate properties may change during the deposition process [4].

The type of treatment mainly depends on the nature of the substrate and the end objective of the deposition process. The substrates can be passive or support materials, the actual object to be protected or functional material. Substrate classification may be based on their levels of crystallinity for instance amorphous, single crystalline and polycrystalline. Other potential classifications, include but not limited to electrical conductivity (insulator, metals or semiconductors etc.), optical and magnetic properties [4]. All these wide forms of classification may bias to what extent and the method adopted in substrate treatment.

The general principle of deposition in thin film technology is that some material (called source material) moves in either gas or liquid phase to form an overlayer on some surface (substrate) for which some desired set of properties can be attained. For this process to occur successfully, most of the source material have to stick on the substrate surface. The most ideal gas phase scenario is that during the deposition process, done under optimal conditions, every particle that lands on the substrates surface sticks contributing to the overlayer or new surface [4].

In real gas phase cases, travelling particles may interact with each other through collisions resulting in modification of momenta. The particles that lose significant portion of their momentum, may fail to reach the substrate while those that excessively gain momentum may reach the surface and fail to stick. The particles may be too energetic and may impinge into the bulk of the material. Alternatively, they may undergo elastic or inelastic collision with the surface atoms leading to scattering (e.g. particle reflection) or heating of the surface resulting in modification of the substrate surface. Therefore, there is always a chance that a portion of projectiles never reach nor stick on the substrate as idealistically intended.

To properly represent these small undertones of the gas phase deposition processes, it is useful to define the sticking coefficient θ. This quantity θ measures the probability that an incident particle, molecule or atom sticks on substrate on impact [4]. This can also be defined from a deposition perspective as the fraction of the impinging atomic species that arrive at and get retained at the substrate's surface [27]. In the case that the incoming particles are of gaseous species, then, condensation coefficient can be used synonymously with θ. In the ideal case, where every incident particle sticks on the substrate surface, $\theta = 1$.

$$\theta = \text{rate of adsorption}/\text{rate of bombardment}$$

The sticking coefficient is affected by a number of factors not only attributed to the incident projectiles to a surface (adsorbent flux) but also on the experimental conditions as well as the nature of the surface itself [4,27]. It is observed that θ decreases as temperature increases, and decreases with coverage due to changes in the substrate adsorbate interactions. In addition, there are disparities in adsorbent-surface pairing. Some materials, even under optimum deposition conditions, have sticking coefficient close to zero for some base surface material, while elements such as copper, gold and silver have sticking coefficient that tend to the ideal case of unity irrespective of the substrate material [27]. Such dependence of θ on intrinsic material properties, temperature amongst others can be useful in fine-tuning a thin film simulation processes.

For the purpose of deposition activities, it is important to look at a collectively covered surface. When an entire layer of the surface atoms is covered with a single layer of film atoms, a monolayer is formed [4]. The number of monolayers can pile up in the event that deposition continues. In this case, the previously formed monolayer acts as the new surface for the next monolayer. Moreover, there is no explicit requirement that the next atomic species must be same as the

previously deposited material. This opens room for numerous combinations of films properties such as expitaxial, pseudomorphic, superlattice films etc.

The above approach based on simply a monolayer gives a good insight on an experimental basis where only final film morphology is important. However, from an atomistic simulation perspective, monitoring of surface structure is most important. Here, surface structure refers to the geometrical arrangement of atoms on the surface and their relative positions to each. Although, the difference is minimal as atomic structure leads to final structure (film morphology). The difference between these two approaches is in the level of analysis. This is so in consideration of the intermediate processes [14].

1.3 Physical Vapour Deposition Technique

Physical vapour deposition (PVD) is a material deposition technique in which source materials in the form of atomic species are transported through physical means onto a substrate (or wafer). The atomic species in essence are vaporized and move through a vacuum or low pressure environment from source to substrate [8, 11]. The general rule of PVD is captured in Figure 3a with the specific case of plasma PVD on Figure 3b. In most PVD processes, there are usually no chemical reactions involved. However, in some special cases the source material may be ionized before reaching the substrate and may react partially with the surface [4, 11].

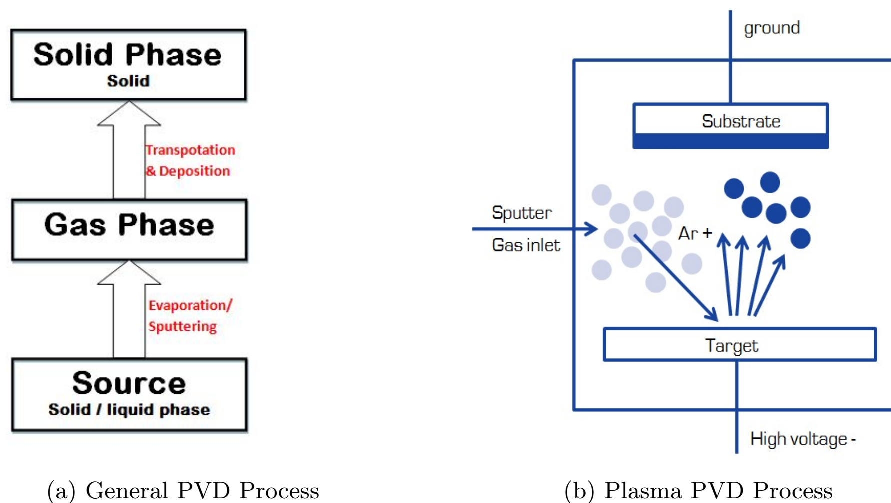

(a) General PVD Process

(b) Plasma PVD Process

Figure 3: Physical Vapour Deposition [10]

The potential applications of PVD are numerous making it a strong rival to other known deposition techniques. This is because of the wide variety of material that can be deposited by this method. These materials include nearly all forms of inorganic materials and some selective organic materials. So far, the application of this technique has successfully actualized films of elemental, alloy, compound and polymeric materials of single or multiple layers. The typical deposition thicknesses are of the orders $\sim 10^{-9}$ m to $\sim 10^{-6}$ m [4, 8]. In addition, PVD is a method of choice over other gas or liquid phase methods since it is environmentally friendlier compared to other methods.

In PVD, there are two common means of moving source materials onto to the substrate. The methods are either through evaporation or through sputtering [4]. At times hybrid processes involving both heating and plasma may be used. For instance, evaporation may be a purely a thermal process but the deposition on the substrate may be aided by plasma of a neutral gas. The most critical consideration on the adoption of the process is largely dependent on equipment available, quality and quantity of film, nature of substrate, cost and skill level of personnel.

In a simulation sense, the heating or plasma technicalities in real experiments can be reduced to particle energies and proper particle types (e.g. ions as particle types). A travelling thermally generated particle, or electric field accelerated particle has some energy. Therefore, a particle could simply be assigned an energy equivalent of an experimental process. In the event that a reaction process occurs as alluded to the reactive PVD, an electron transfer mechanism could be used to represent such a process [4].

In setting up particle energies, a rough idea of the physics of atomic condensation and collisions should be considered. This ensures fairly good approximating of energies ranges, and reasonable predictability of key film properties (such as surface texture, grain properties (size and morphology), defect and stress) that change as a function of deposition energies [4]

For instance, condensation of atoms from vapour phase releases latent heat of condensation. This heat induces localized heating of the substrate's atoms. Depending on the deposition energy, the aftermath of condensation can range from minute localized vibrations to ejection of surface atoms by evaporation. Further, assuming that no evaporation occurs, then sufficient energies on impact can also induce elastic effects. The elastic effects can lead to shuffling of surface or near-surface atoms. This rearrangement can induce film stress, lead to a smoother film surface or generate surface defects [4].

1.4 Film Uniformity and Conformality

PVD is a powerful film deposition technique. However, it is not flawless in the sense that it presents challenges with respect to film uniformity and conformal coverage. By uniformity, we refer to the film thickness across the substrate surface in the direction perpendicular of the source material generator. Conformality refers to the sense in which trenches on the substrate are filled by the film over the deposition process [4, 8]. This deposition method has technological interest in the aspect that it can be used developing functional materials. Therefore, other than just performing a random deposition exercise, consideration of both conformality and uniformity is important as it directly influences the quality and use of the final product.

PVD is a line of sight technique [4,8]. This loosely translates to the source material(s) reaching the substrate surface without collisions. This is positive in the sense that coverage is always close to unity for a reasonable size of substrate. On the downside, uniformity of source material deposited in some fractional area of the substrate depends on the geometry of source to substrate. This is illustrated in Figure 4, where h and r are hypothetical distances defined between the source and substrate [4, 8].

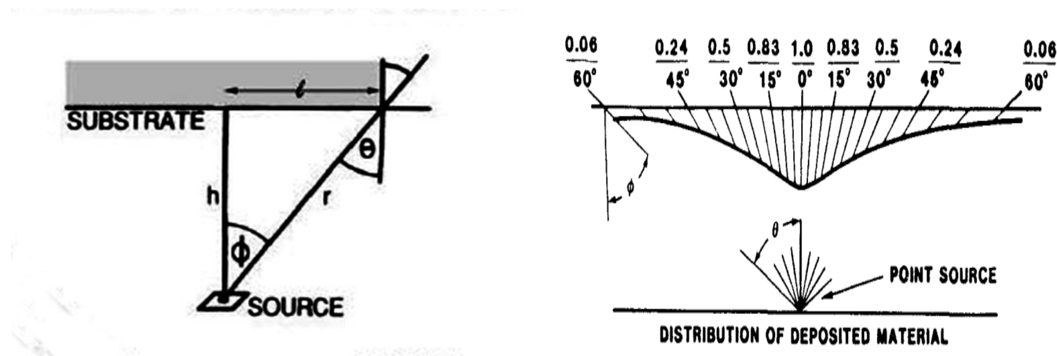

Figure 4: Effect of source-substrate geometry on uniformity of deposition [4, 8].

It can be seen that the distance travelled by the flux depends on the angular projection of the flux from the source holder ϕ and the orientation of the substrate θ. These two orientation parameters affect the time taken by evaporant flux to arrive at the substrate from the source holder. Therefore, areas in the direct proximity of the perpendicular distance h get thicker faster that those areas for which $r > h$ [4, 8]. It can be seen that from Figure 4 in the range $0°$ to $60°$, the film thickness changes from 1 - 0.06 deposition units (thickness per unit time). This non-uniformity, for instance, can generate errors in resistance estimation in electronic microchips.

Geometry dependence is not a permanent weakness in PVD. The film distribution is not linear but radial. This means that there are always areas that have equal film distribution. For instance, if we imagine having a semicircle, then all areas defined along the radius will have equal distribution of material (uniform deposition). Therefore, having a curved substrate along the radial flux tract can actually mitigate the effect of geometry [4]. This reasoning assumes that other factors such as the flux rate are constant. In actual PVD, melting and evaporation of source material interferes with the angular distribution of evaporant flux. This is because the depth on which the source material emerges from the crucible (or source material holder) changes as evaporation progresses.

A practical solution to this problem can be illustrated by considering highly directed flux and the case $l \to 0$ (Figure 4). This is interpreted as the case for which the area of substrate deposition is very small. Geometry dependence disappears or is minimal. To practically achieve this, it is required that the distance h be very large in the limit that the flux angle dependence is diminished [4]. However, it is not necessarily true that a small substrate is desired at all times.

Another means of dealing with the geometry problem is to eliminate orientation dependence i.e. deal with θ & ϕ. This is practically implemented by rotation of the substrate in planetary motion. This ensures that $r \to h$ at any instance during deposition or the difference in the flux in linear flux tract is compensated for [4]. The challenge that normally arises in equipment flexibility.

A number of ways to improve uniformity have been mentioned. However, the individual methods employed in the deposition processes may yield different levels of uniformity. For instance, the close proximity of target and substrate in plasma processes produces much better uniformity than evaporation by heating processes. Collimation of plasma sources may be adopted in preference to direct the ion sources. There is always a restriction of the equipment flexibility and wastage of source materials that may require extra attention.

In PVD, film conformality just like uniformity is usually poor. Trenches and terraces have high likelihood of being filled with voids [11]. The fundamental reason is that the technique is a line of sight deposition technique. This means that areas in which the deposition progresses faster outgrows other less favoured areas.

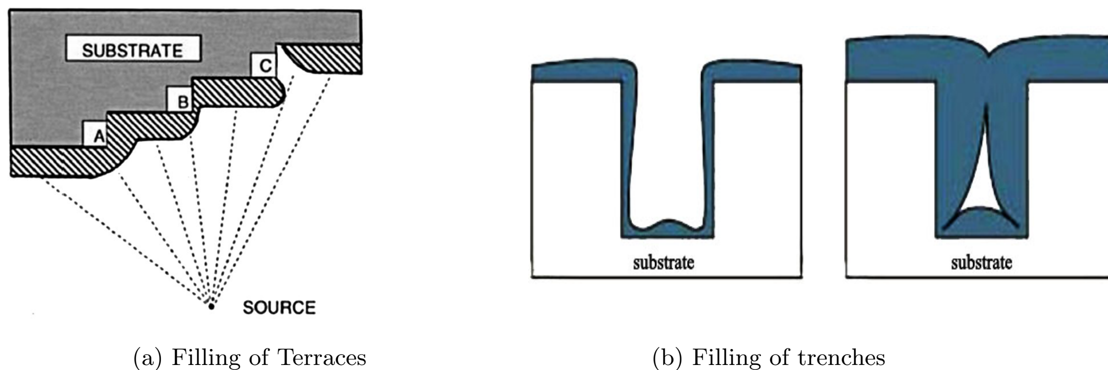

(a) Filling of Terraces

(b) Filling of trenches

Figure 5: Conformal coverage in PVD

The nonuniform growth rate is primarily a problem of geometry, but the crux of poor conformality is shadowing of the adjacent areas [11]. In Figure 5a, Area A has relative uniform deposition while C has almost no film coverage due to shadowing. If the film growth progresses, then, area C will have a void [4]. This is captured in Figure 5b, where a void is clearly visible on the filled substrate.

Similar solutions as those of uniformity problems may be applied to combat problems of conformal coverage. However, this is still a great challenge as the problem of conformality increases with down scaling. Despite this, any method that can enhance surface diffusion of adatoms such as heating the substrate or deposition at high energies, to a great extent, will eliminate or reduce this challenge.

1.5 Ion Beam Assisted Deposition

Ion beam assisted deposition (IBAD) is a special form of high vacuum PVD process in which film deposition happens through two separate but simultaneously occuring events. In this technique, normal deposition of PVD takes place and an additional bombardment of the deposited film by ionic species is implemented. In respect of surface deposition, the typical range of bombardment energy is 0.1-30 keV. Higher energies can result in damaging of the film overlayer [28]. The key point that distinguishes IBAD from other plasma PVD techniques is the requirement of a separate bombardment sources during the deposition processes. This means that the film forming material is generated from a different portion of setup to the bombarding ion source. This form of setup is illustrated in Figure 6 [28, 29] where generation of film forming material (either by evaporation or plasma) is isolated from the ion bombardment part.

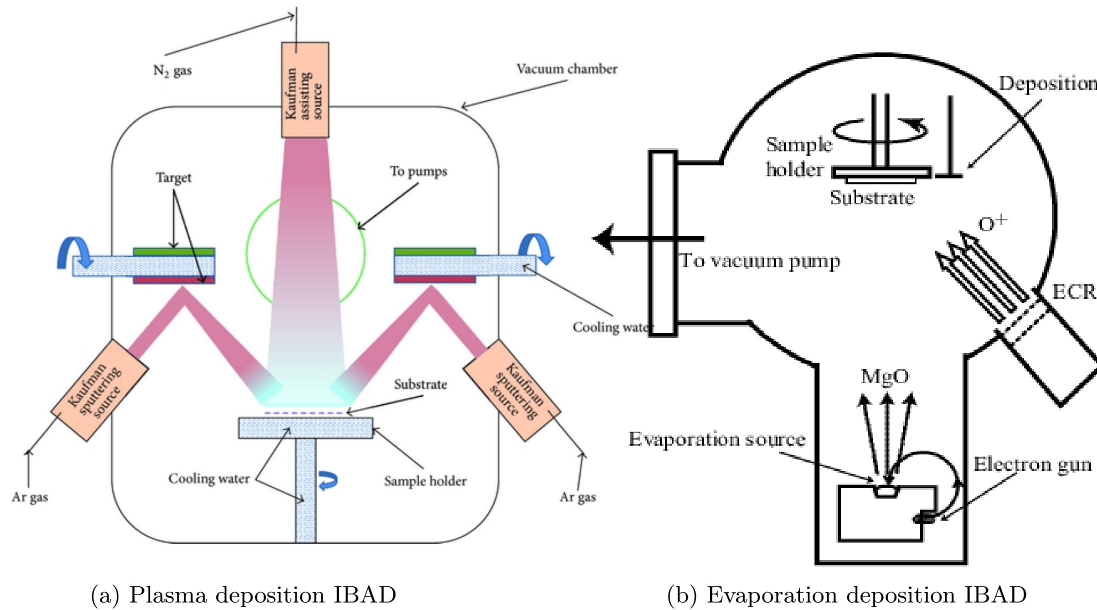

(a) Plasma deposition IBAD (b) Evaporation deposition IBAD

Figure 6: Deposition by using IBAD [29, 30]

The bombarding ions are controlled independently of the deposition process. This gives room for determing the number of incoming ions, angle of bombardment, kinetic energy of ions, and periodicity of the bombardment amongst other. These control parameters are necessary in influencing the kinetic energy transfer during bombardment process and by extension activation of surface processes. Therefore, the bombardment in one way or another influences coating stoichiometry (especially with reactive IBAD in which a reactive gas such as oxygen is used instead of argon), microstructure and film stress. However, the two most dominant factors that influence the final

film structure are the bombardment energies and the ion bombardment to deposition rates (also called ion-to-atom rate or ion fluence) [9].

Ion bombardment in IBAD process can be done simultaneously or alternately with the film deposition. Simultaneous bombardment of ions requires low energy sources with no mass separation while higher energies are appropriate for alternate ion bombardment. The exact energy required for the latter process depends on the thickness of the film layer deposited [28].

The motivation of using IBAD as opposed to PVD is that it produces better films in terms of densification. In PVD, effects of line of sight deposition such as voids and vacancies are mitigated by the bombardment cycle. In this cycle, transfer of momentum occurs providing a source of mobility of atoms across the surface and partial surface damage generates heterogeneous nucleation. The destabilization of surface atom clusters promotes step flow growth and formation of layer-by-layer growth. Moreover, IBAD allows growth at much lower temperatures. This implies that film deposition can be done at low energies (~ 0.1 eV) provided that there is a substantial bombardment energy [9].

Ion bombardment is complex phenomena. Despite the aforementioned improvements that IBAD offers to PVD, a haphazard approach to IBAD may negatively influence the film structure and other film derivative properties such as grain properties, film adhesion, topography, stress and defects. For instance at high energies, bombardment may tamper with bulk properties of the substrate. In addition, at relatively sufficient energies, if the rate of bombardment is excessively high, the process may shift from a deposition to sputtering process. Therefore, at all times, the setup must always ensure that there is net deposition or film growth [4,22]. The easiest implementation is the one involving an alternate bombardment and deposition cycle.

1.6 Growth Modes

In different applications of thin films, it may be desired to have different surface or multilayer surface properties. One of the possible ways of achieving this objective is by controlling the energy of the incoming particles, substrate conditioning and experimental conditions (mostly pressure and temperature at film growth). The substrate properties are more or less independent of the deposition process because they can be controlled to a great level of precision.

In consideration of particle energies, for low energy particles, the type of film formed may be explained by using the classical growth modes. However, it is been observed that at energies of $\simeq 20$ eV surface defects such as short-lived vacancies start appearing on the film. For higher particle energies $>> 30$ eV sub-plantation starts to occur. Therefore, the deposition is no longer purely on the surface but also on the subsurface [22]. Growth on subsurface in one way or another has varied influence on the surface depending on the material being deposited.

There are three common classification of film growth modes that results from a deposition process. They are in some context referred to as classical growth modes [22], and the manifestation of any of three modes depends on a number of factors inclusive of the interface energies between the adsorbent particles and substrate, lattice parameter mismatch between film and substrate, incoming flux rate of adsorbent and growth conditions (e.g. temperature). The modes are:

- Layer by layer growth or Frank van der Merve (FM) growth mode
- Layer by island growth or Stranski Krastanov (SK) growth mode
- Island growth or Volmer Weber (VW) growth mode

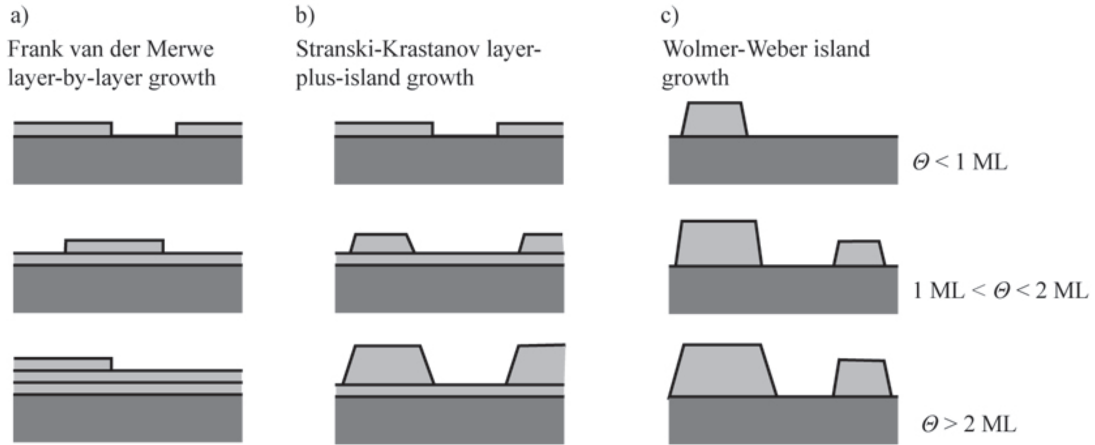

Figure 7: Growth modes in PVD process [23]

In the growth of epitaxial films, elastic strain accommodates interfacial differences in the atomic spacing between thin film and substrate (also called lattice mismatch). In a plain description, after the first few film monolayers' lattice spacing is coerced to match that of substrate. In the event of a few monolayers, and perfectly flat surface with no special sites, the over layer can be assumed to be coherent with the substrate. The growth will be pseudomorphic i.e. first monolayer of adatoms will adjust and adopt the in-plane lattice constant of substrate. As the number of subsequent monolayers increases growth proceeds layer by layer. However, after a critical thickness of deposited film, defects starts to appear along the film-substrate interface or within the growing film [4]. This is the elastic theory of epitaxial growth and it is the basis from which FM growth mode is initially conceptualized [31].

VW growth has its roots in nucleation theory. The driving force behind the formation of three-dimensional (3D) islands is the relative strength of the interface energy and surface free energy. The mixed growth mode (SK) presumes the existence of a few pseudomorphically grown monolayers on a substrate on which 3D islands having the original lattice constant of the adsorbate grow. This model was developed from atomistic calculations [31].

To gain a holistic insight to the classical growth models, more unified formulations are developed based on the thermodynamics or kinetics of the process involved. In the former, the attention is fixed on the final form (film morphology) without necessarily paying attention to the intermediate structural activities. In the latter, sizeable attention is accorded to the intermediate steps.

1.6.1 Thermodynamic model

In conditions close to or at thermodynamic equilibrium, the minimum energy film morphology can be easily described purely on thermodynamic considerations. To visualize this, a liquid drop is used analogously to a film nucleus. The contact angle made by the liquid drop onto a surface is controlled by surface tension and wetting surface energy. The interplay between these two energies dictates the phobic behaviour of the liquid drop. It is observed that a greater contact angle made by a liquid droplet onto a surface corresponds to a low wetting activity (or phobic behaviour) [4].

In thin films, a similar argument holds but with slightly different definition of the energies. In this respect, the equilibrium appearance and structure of film from a deposition process is mainly governed by the direct "competition" between the surface free energy required for additional surface formation and the interface energy. The various surface and interface energy of film and substrate are defined as γ_0 is the over layer and vacuum interface, γ_i is the over layer and substrate interface, and γ_s is the substrate and vacuum interface (see Figure 8) [4, 17, 23].

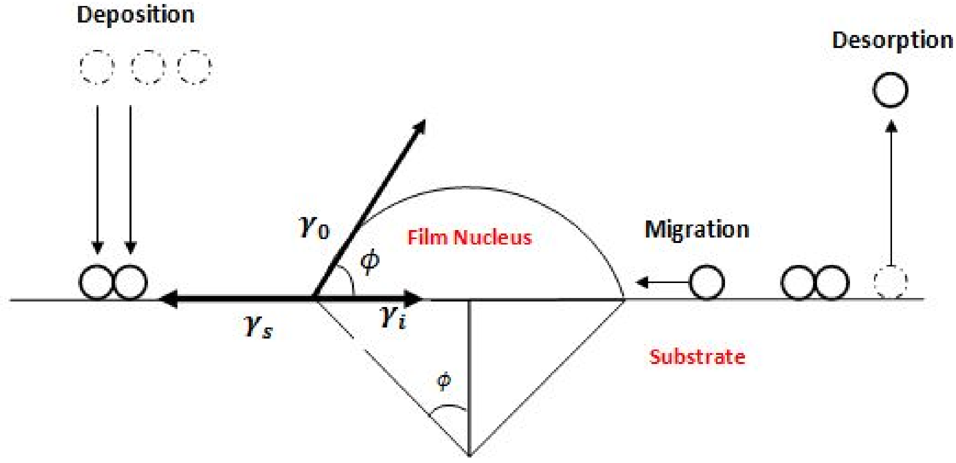

Figure 8: Film formation in heterogeneous nucleation process [23]

Using the above definitions, the equation governing the appearance of the final morphology can be expressed as:

$$\gamma_s = \gamma_i + \gamma_0 \cos\phi$$

Here ϕ is the wetting angle. The interpretation can be easily be shown by accounting for the two extreme cases such that:

$\phi > 0$	$\gamma_s < \gamma_i + \gamma_0$	island growth (VW)
$\phi = 0$	$\gamma_s \geq \gamma_i + \gamma_0$	layer by layer growth (FM)

In the intermediate (SK) growth mode, the initial condition for FM is met. However, lattice mismatch between film and substrate forces the film to adjust to the substrate's lattice constant at the expense of elastic deformation. The initial monolayer is slightly affected by the deformation. However, as deposition continues, the magnitude of the elastic strain continues to increase. At the point for which strain energy exceeds the magnitude of adhesive forces of the deposited material, formation of islands becomes inevitable [14, 23].

The equilibrium conditions also apply to the whole deposition system. Therefore, consideration is accorded to the vapour pressure on both condensed and gas phases. This relation can be captured by monitoring the change in Gibbs free energy ΔG. At equilibrium vapour pressure $p_0(T)$ (T is temperature), $\Delta G = 0$. However, changes in the particle number n from the vapour phase to solid phase at some pressure p changes ΔG. This is a direct consequence of change in free enthalpy [14]. Therefore, a full deposition outcome should include Equation 5 as its extension. For example $\gamma_s < \gamma_i + \gamma_0 + \Delta G$.

$$\Delta G = nk_bT \ln p/p_0 \tag{5}$$

The justification of this model lies along experimental observations. In an experimental setup, we observe the final morphology (film /surface) after deposition as opposed to the intermediate steps.

1.6.2 Atomic model

All vapour deposition techniques are non-equilibrium processes [22]. This is partly due to the inability of the deposited material to rearrange itself instantaneously to minimize surface energy. Therefore, the deposited film properties primarily depend on deposition conditions. The factors that significantly affect film properties are type and energy of depositing species, type and temperature of substrate, and deposition rate [22].

In non-equilibrium conditions, the nature of the substrate's surface becomes very significant [17]. This is because the sticking (or condensation) coefficient actually depends on the nature of surface sites. It has been shown that, at low supersaturation (p/p_0 as defined in Equation 5) where diffusion lengths are much smaller than surface step sites, the sticking coefficient is unity. This translates to growth that is meditated by defects. At higher supersaturation, adatoms cluster together before reaching the surface. When adatoms land on the surface, the difference between their cluster binding energy and the surface-adatom energy determines whether they form a nucleus for the formation of islands or not [17]. Therefore, a more elaborate model has to be formulated to address such realities.

The atomic model focuses on the interaction of the individual adatoms as opposed to a film overlayer (monolayer) presented in the thermodynamic model [32]. It addresses the deposition from a general condition in which the states of equilibria are not of central importance. It starts by acknowledging that ideal smooth flat surfaces do not exist, i.e. there always exists few mishaps on surfaces. The defects at surfaces are not that bad after all as illustrated above. Moreover, this model approaches film growth from a simulation angle in the sense that it slows down the deposition process to analyze finer details of deposition. Thus, it is more of a step-wise deposition approach.

If we define the the surface-adatom interaction energy as γ_b and that of an adatom-adatom interaction as γ_a, this model predicts that [32]:

$$\gamma_a \geq 3\gamma_b \qquad \text{layers by layer deposition}$$

$$\gamma_a \leq 3\gamma_b \qquad \text{Island deposition}$$

The SK mixed mode has no single expression like the two diametric forms of deposition. However, it is a result of subsequent deposition due to change in the underlying surface. After the first monolayer of atoms have been deposited and adopted a layer-by-layer outlook, the new surface is no longer attributed to the initial substrate. After the initial monolayer, island growth occurs as the 2nd, 3rd ... monolayers are actually surfaces formed by the adatoms (same species). Therefore, we have a case of an initial layer-by-layer deposition followed by island deposition.

1.7 Columnar and Grain Growth

The two main concerns during film growth are porosity and roughness. These factors are most important in areas where performance and reliability are of great concern [18]. For example, a rough interface can be a source of amplified electric field or an optical scattering centre. The questions is rather of the implications of such attributes on intended applications. If they are intentionally designed, they can be used for the better good. On the contrary, self-mutation of surface or interface can lead to failure or be the source of killer defects in microelectronics. Two of the many driving forces that mainly influence (surface) roughness of thin films are temperature and grain growth. Temperature has far much implication as it influences diffusion, nucleation, desorption and therefore to some extent grain growth [18]. However, incorporation of ion bombardment or any other process that initiate rapid film kinetics during or after deposition can produce similar effects to those implied by temperature.

The temperature stability and magnitude during and after deposition processes has direct ramifications on film microstructure. Alteration of equilibrium dynamics and processes such as diffusion are (partly) ripple effects of deposition conditions. Narrowing down to temperature and assuming high deposition rates, the range of temperature T_i determines the final morphology and classification of film. For example, in the case of metals, the outcome can be summarized by the temperature relation $0 < T_1 < 0.3T_m < T_2 < 0.45T_m < T_3 < T_m$ such that T_m is the melting point of the metal. At Zone I (T_1), the film is porous, Zone II (T_2) the film is made up of columnar grains that are separated by metallurgical grain boundaries, and Zone III (T_3) equiaxial grains dominate the film [16]. These film zones are clearly captured in Figure 9. The temperature definition of the zone model is known to vary from material to material [16, 18].

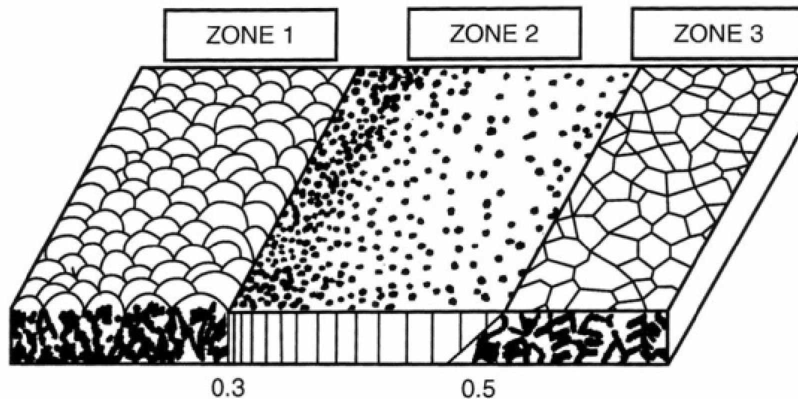

Figure 9: Zone model for metallic structure [18].

Film growth in one way may be thought of as a sequence of nucleation, coalescence and thickening processes. In the formation of islands through nucleation, the islands grow as result of adatoms being integrated at the perimeter of the nucleation site. The growth is actually a contribution of both adatom from vapour phase and surface diffusion. This makes film growth dependent on both deposition rate and diffusion (indirectly temperature T). The former contribution is obvious but the latter has hidden implications. Assuming that deposition stops, nucleation process will still take place. To illustrate the temperature T contribution, we define the energy of formation of a cluster of some size n as ΔG_n, then, the nucleation rate I can be crafted as:

$$I = I_0 r^* \exp\left(\frac{-\Delta G}{kT}\right) \tag{6}$$

Here, I_0 is a constant and k is Boltzmann constant. Supersaturation decreases with increasing temperature or from the equation ΔG increases with increasing temperature. Then, the nucleation process is completely dominated by temperature contribution at higher temperatures [18].

The growth of clusters and islands is limited by a critical (size n) - or for the special case of spherical shaped clusters radius r^* - for which deviation attracts instability. The critical radius can be defined as $r^* = -2\gamma_f/\Delta G)$ [18]. In addition, there are specific orientations that are given preferential growth. The critical cluster size (or radius) and orientation are driven by the requirement of minimization of both surface and interface energies. Violation of this simple requirement is accommodated by metamorphosis of islands, whereby segregation of oversized clusters or size increment of cluster through aggregation of smaller size clusters.

The mutation of the various sizes of the clusters or islands is not the most crucial aspect informing smooth continuous film. The term smooth means a very low degree of roughness on a continuous film. The clusters grow also in the lateral directions relative to the substrate's interface. This lateral growth leads to coalescence. Coalescence means that two stable adjacent islands come into

contact with each other. The interface of these two coalesced islands undergoes transformation that intends to reduce further the interface energy. This newly formed interface is a grain boundary. Thus, coalescence leads to the formation of grain boundaries

The coalescence process may not necessarily results in same size grains. This leads to grain growth. In grain growth process, what is observed is the apparent shrinkage and elimination of smaller grains. However, the actual modality of this growth process is that grains of low surface and interface energy have preferential growth rate. Therefore, even the assumption of equally sized grains does not invalidate grain growth. Assuming the existence of a defect free film having grains of spherical shapes with an average in-plane radius r, the average grain growth rate represented as dr/dt is proportional to the average change in the curvature κ of the grains [18].

$$\frac{dr}{dt} \propto \frac{m\gamma_{gb}}{r} = m\gamma_{gb}\kappa \text{ where } m = m_0 \exp(-Q_{gb}/k_b T) \tag{7}$$

Here, γ_{gb} is the grain boundary energy, m is the average grain boundary mobility, m_0 is a constant, Q_{gb} the activation energy, T is temperature and k_b is Boltzmann's constant. High temperatures favour rapid mobility and hence the process hastens, however, it is not a requirement. The reason is that the grain growth process is primarily a self-driven process aimed at reaching a system's equilibrium state. Provided that the system is not frozen at 0 k, temperature is a secondary process in grain growth.

The path to equilibrium entails driving the grain boundary energy to a minimum value. Deducing from Equation 7, reduction of grain boundary energy would require a reduction of the curvature (reciprocal of average radius). The interpretation is that, as grains grow (or average radius increases for spherically shaped grains) the grain boundary energy is reduced. In general, what is observed is that the grain boundary length per unit area of the film is reduced. This is captured in Figure 10 where the original radius R (of the model grains) marked with the dashed lines has been deformed. The shape of two initial coalesced islands have been transfigured.

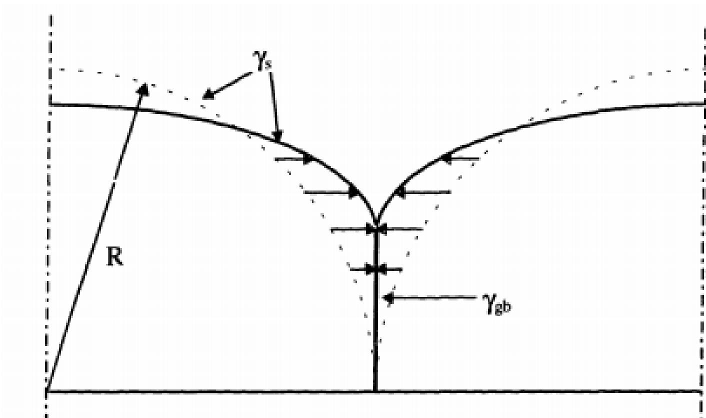

Figure 10: Grain boundary distortion [18].

In the absence of any form of diffusion, grain boundary relaxation leads to development of strain in the coalesced islands. At this stage, stress also develops on the film as result of density deficit of film relative to the bulk. These two problems are accommodated by smaller grain sizes at the coalescence stages. However, in the case where diffusion is permitted, the resultant shapes during grain boundary relaxation adopt fixed volume equilibrium shapes. In the event, that there exist substantial differences in the interface or surface energies, there can be a complete merger of two islands whereby one is incorporated into another [18].

Continuous grain growth and grain boundary evolution and dynamics leads to thickening of film. The thickening leads to formation of columnar structure with relatively uniform thickness and restricted roughness. This is what is seen in the Zone model as Zone II. Actually, this process is driven by growth velocity, surface energy and strain energy anisotropy. The velocity aspect can be achieved through either allowing thickening to happen at low temperatures and follwed by annealing of the film. Alternatively, thickening can be done at high temperature leading to large columnar structures (or equiaxial structures) [18]. The temperature chosen for thickening depends on the materials. For some materials thickening of grains is not possible at high temperatures. In a simulation sense, this can be seen as reordering of atoms at various section of the film.

1.8 Energetic Particles

Assuming that a particle within a system has kinetic energy of the same order of magnitude as the average energy of all the particles in that system, the velocity associated with that particle is called thermal velocity.

Energetic particles of atomic species (i.e. neutral atoms, ions, small molecules or clusters) are particles whose energy is much greater than the thermal velocities [4,22]. Irrespective of how they are generated, they have the ability to form film on a substrate (surface deposition processes), penetrate slightly below the substrate's surface into a few monolayers below the surface (particle sub-plantation), or penetrate deeper into the substrate's bulk (implantation) [22]. All these possibilities on a material substrate can be attributed to the energy of the particles. In addition, complex phenomena such as partial or complete momentum transfer from incident particles may result in heating of the substrate, strain and texture modification and chemical potential modification [22].

The source particles can be described as thermal, hyperthermal or accelerated [22]. The energies associated with the particles are tabulated in Table 1. Their level of interaction for any energy classification is both clear and vague. This is because certain surface and bulk activities occur within overlapping energy classification ranges while others are within specific ranges (Figure 11). For instance, energies greater than 100 eV favour bulk processes (deposition, bulk defects) and as well as few surface processes (like surface erosion). These variations and their probable outcome are captured in Figure 11. Despite the existence of such conundrum, it is more or less observed that thermal particles promote deposition processes, hyperthermal particles cause sub-plantation while accelerated particles cause implantation [22].

Particle Classification	Energy (eV)
Thermal	< 1 eV
Accelerated	> 1000 eV
Hyperthermal	1eV $\leq x \leq$ 1000 eV

Table 1: Classification of particles based on energies

The subplantation and implantation phenomena at face value appear to be irrelevant to classical growth modes. However, this is not the case. Surface or subsurface alteration influences the nature of classical growth mode through strain, stresses or defects. In addition, processes like implantation (high energies $\geq$ 100 eV), have potential of forming voids and nucleation sites [22]. These processes alter atom embedding energies on the surface and are more pronounced at surface bulk boundaries. Thus, the observed surface profile is no longer exclusively dictated by the surface but partially by the bulk.

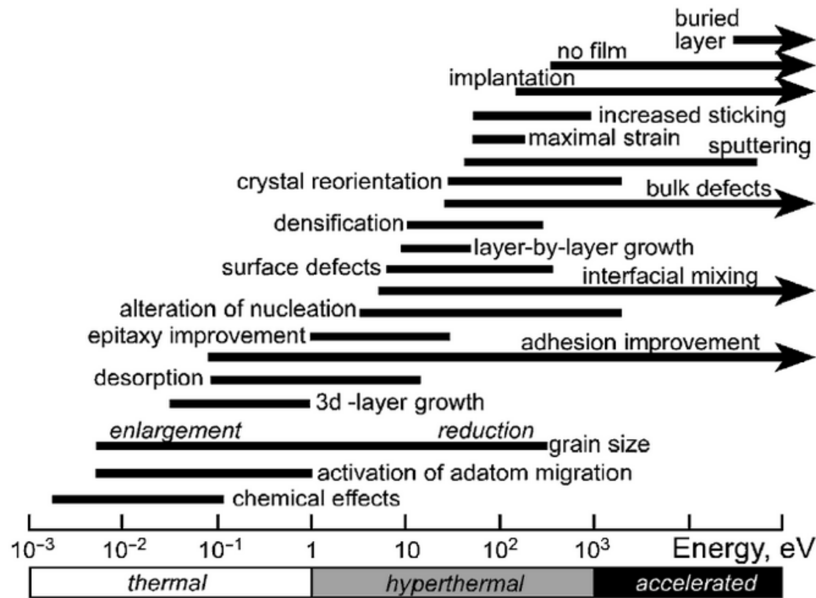

Figure 11: Particle-substrate interaction energy ranges [22]

1.9 Applications of PVD

Coatings of PVD can be broadly classified as functional or decorative [4]. PVD can generate a very broad range of coloured coatings, and therefore makes it an ideal means of decorating materials. Many products inclusive of kitchenware (knives and spoons), musical instruments, bath fittings, door handles and jewellery of all kinds have been subjected to PVD decorative process.

In functional coatings, the coatings are applied to improve or tune a material's mechanical and chemical properties, electromagnetic response amongst others. A single or multiple underlying properties such as hardness, thermal stability, and chemical attack resistance may be targeted to achieve the required function. Examples include medical implants, tools (drilling, cutting, and moulding) and aviation accessories (compressor blades for jet engines). In other cases, both decorative and functional properties may be applied at the same time using the same coat. For example, watches can be coated such that they attain the shiny aesthetic quality but at the same time attain protective properties of the underlying material against chemical attack (oxidation) and mechanical wear [4].

In the semiconductor and microchip industry, PVD is both a primary and secondary method for deposition. Primarily, it is used in fabricating integrated circuits mainly in ultra-thin cap and seed layers for both interconnects and metal gates in advanced transistors that utilize high-k gate materials. The secondary role is in the processes of film patterning and etching processes. Most masks are prone to damage by etching agents. PVD provides a means of depositing "hard masks" such as of those of TiN. Such masks ensure that the underlying film layer is properly protected during etching processes [24–26].

Zinc Oxide (ZnO) is a semiconductor material with a direct bandgap of 3.32 eV. It can be processed in the nanoscale to make laser diodes and ultraviolet sensors. Traditionally, the process of making high quality ZnO nanoproducts required high temperatures for which many substrates would not survive. This limited substrate selection and by extension functionality. PVD provides a means of manufacturing such nanoproducts (rods, wires and belts) at lower temperature. The use of low temperature deposition in PVD, allows room for a wide selection range of substrates [25].

1.10 Modeling PVD

In PVD, source material can be generated by either evaporation or sputtering. This makes the approaches different by experimental design. Moreover, each individual approach is very complex and hence independent solutions are needed to address the various components constituting an experimental setup [4]. Therefore, simulating such a process would be best approached by segmenting the various components or stages of a deposition process. Although the umbrella algorithm summarizing the deposition process may appear to be simple, it is made up of different algorithms for each stage, i.e. simulation algorithm is an aggregate of separate algorithms. In cases that involve plasma sources or in IBAD, the plasma generation may be considered as a separate part of the setup. Thus, the simulation starts from the point at which the plasma gas is already present.

The three steps that occur in PVD processes are flux generation from a source, flux propagation between source and substrate, and finally the flux deposition on substrate to form a film. This can be taken further by adding a fourth step that include microstructure or morphological dynamics and evolution of deposited films [4]. The stratagem of this thesis is narrowed down to flux propagation from source to the point of deposition. Post deposition and other complex phenomena are ignored. Moreover, a good portion of the argument to be presented here leans on cosine model of flux propagation. The cosine model is an approximation of the real system [4,11], and more so the line of sight nature of PVD allows for its use.

The first assumption is that projectile flux have linear trajectories irrespective of the method of deposition chosen (vaporizing or sputtering) to simply analysis. This is illustrated on the small point source in Figure 12. However, this is not true for real evaporant flux projectiles. The situation is worse for plasma sources since the targets of erosion are never small [11]. This makes every point struck by incident particles a point source. In Figure 12, the amount of possible intersection (collision) of projectiles from the planar source clearly illustrates the weakness of this assumption [11]. The amount of trajectory modification would be too cumbersome to formulate or impossible to deal with using a deterministic approach.

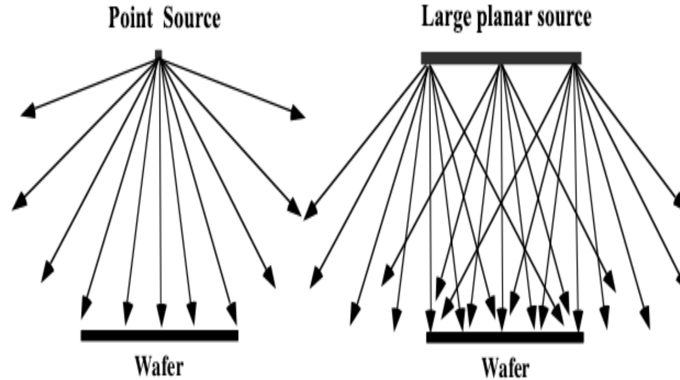

Figure 12: Flux direction from a sputtering target [11]

Despite this, linear trajectories can be justified because the vapor pressure at the source (crucible) is always higher than the ambient scattering sources. In addition, most PVD processes are done in some form of vacuum environment that ensures longer mean free paths of atoms in gas phase [4,11]. However, this does not mean that no inter-particle scattering occurs nor is the linearity of paths always guaranteed. The net effect is that the undesired features associated with real systems, such as non-linearities, are never too adverse to prevent PVD process from taking place. This is true since deposition is still observed in experimental setups. Therefore, it is justified to assume them.

Flux emitted from a point source has a wider-angle distribution. To model this case, the only consideration is the emission angle θ_i relative to the wafer. In contrast, a wider planar source can be argued to be emitting source material in the same manner as multiple adjacent point sources each with its own emission angle. The emission angle θ_i must therefore be defined widely to cover all possible 'point sources' constituting the small planar source. These two scenarios are shown in Figure 13.

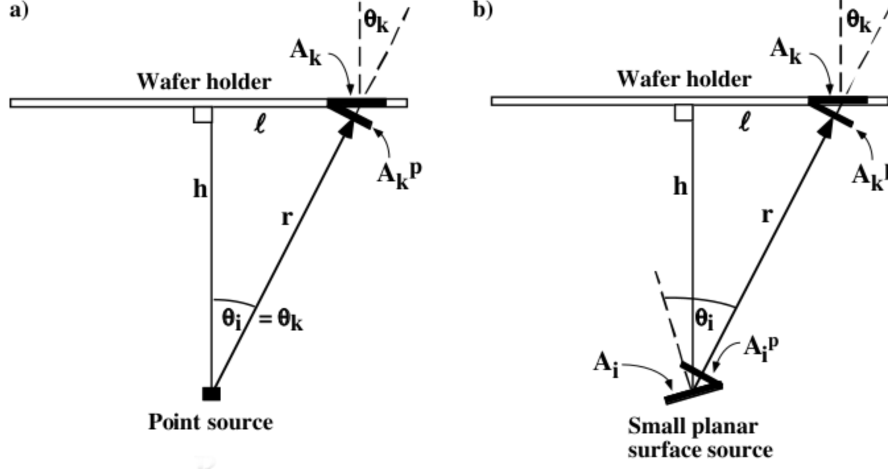

Figure 13: Point and small planar sources in PVD [11]

We can define fluxes F_o and F_s as fluxes from the source and to the substrate surface respectively. F_o is the mass of evaporant leaving the source (crucible) and is radially emitted per unit time while F_s represents the flux reaching the substrate surface per unit time [11]. These fluxes for both point and planar sources can be represented as:

Point Source	Planar source
$F_o = \frac{R_E}{\Omega r^2}$	$F_o = \frac{R_E}{\pi r^2} \cos^n \theta_i$
$F_s = \frac{R_E}{\Omega \rho r^2} \cos \theta_k$	$F_s = \frac{R_E}{\pi \rho r^2} \cos^n \theta_i \cos \theta_k$

Where θ_i and θ_k are angles defined with respect to the outward flux and deposited flux respectively (see Figure 13). R_E is the evaporation rate, ρ is the density of the material deposited, and $\Omega = 2\pi$ is the half solid angle representing flux ejection in the upward direction only. The index n in the equation of the planar sources defines the level of isotropy of emission from the source without consideration of substrate position. When $n = 1$, this is the case of an ideal cosine emission from a small planar source. A similar argument relating to n holds for arriving flux on some small substrate surface [11].

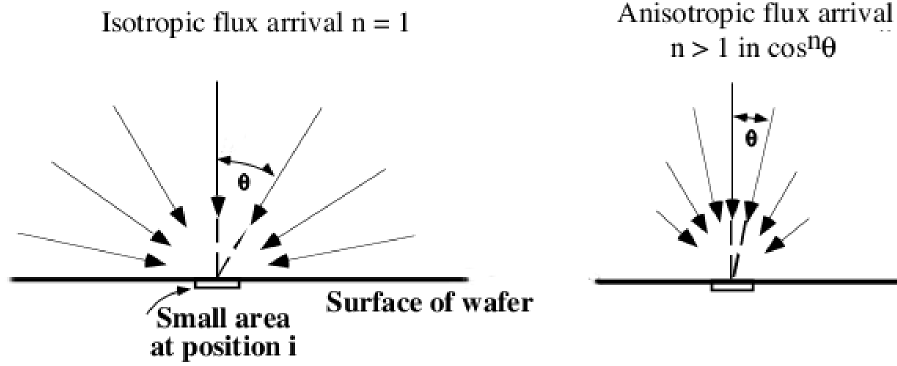

Figure 14: Flux arriving at the substrate surface at different angular distribution [11]

The flux arrival onto a substrate can be either anisotropic or isotropic (as capture in Figure 14) depending on the size and orientation of source, and distance from source to substrate. Assuming a constant flux production rate and a relatively small flat stationary substrate, and a substantial distance between substrate and source, radially emitted flux from a source would mean anisotropic arrival of flux on the substrate. This implies that less deposition per substrate unit area in every deposition cycle. Using multiple adjacent point sources (or a small planar source) would translate to an improvement net deposition and improved isotropy per substrate unit area. However, still additional geometrical considerations have to be considered.

Modelling of the surface processes can either be considered purely based on deposited flux, or on the surface influence on the flux deposited. With respect to flux, we can consider effect of flux rate on adsorption and desorption processes while in a surface controlled process, we take into account the effects of surface energetics and topography on deposited flux [11]. However, in the full description of the events happening at the surface during deposition more factors can be included.

At constant flux rate and a perfect surface, growth on the surface depends on flux that directly lands on the surface F_s. The direct flux is expressed as $F_s = F_0 \cos^n \theta$, where F_0 is the final projected flux towards the surface and the angles can be inferred from Figure 13. This is the direct flux that can be adsorbed, scattered off or undergo desorption after adsorption. Therefore, we narrowly define the sticking coefficient S_c as the fraction of direct flux that is adsorbed on the surface [4, 11]. The primary deposited flux F_d is dependent of S_c such that $F_d = F_s S_c$. and film growth must include surface conditions and properties. Therefore, the net-deposited flux on surface F_{net} is now defined in some complicated equation:

$$F_{net} = \frac{D_s}{k_b T} \gamma_s \Omega \nu \frac{\partial^2 \kappa}{\partial s^2} F_d C_s + F_d \tag{8}$$

Here, D_s is the collective surface diffusion coefficient, T is the surface temperature, γ_s is the term representing surface energies which also includes aspects such as, crystallographic planes, special sites on surfaces(kink, terraces, ledge, vacancies) etc., Ω is the adatom's volume, ν is the surface atom density, κ defines surface curvature, s unit length travelled along the surface by an adatom, and C_s represent other substrate's constants [11]. Nevertheless, this seemingly complicated equation in its contracted form may have additional terms, for instance in the case of IBAD, where the bombarding ion energy may induce desorption (or sputtering), surface temperature variation, enhanced surface diffusion etc. which must be accommodated in the model.

2 Molecular simulations

2.1 Introduction

Computer simulations provide an alternative means of testing or visualizing physical phenomena. This is because there are certain phenomena that can only be captured through simulations. On the other hand, simulations act as bridges between theoretical and experimental work. This is the sense that a well-developed theoretical model can be easily be tested by a simulation. Afterwards, the result of the simulation is juxtaposed against experimental results for validation [5]. The reverse engineering of experimental results can also be used to develop a proper theoretical model. Since simulations can probe some blind sites of experimental observations, a sketchy theoretical model can be improved. Flexible techniques inclusive of fixing parameters, parameterization or even guessing some inputs or parts of the system can be implemented during the bridging process. These aspects make simulations flexible and powerful tool in developing models and testing phenomena.

In scientific simulations, a physical phenomenon is translated to a computer program or (a set of) executable code(s). This process involves implementation of an algorithm or series of algorithms to reproduce and explore the limits of the phenomenon under investigation. The main objective of such a rigorous process may be to monitor the dynamics, obtaining new or testing old parameters, calculate properties of the systems etc. [5].

The methods used in simulations include Monte Carlo (MC) techniques, Molecular Dynamics (MD) and *ab initio* methods. There is no simple bias to the selection of modeling style to be implemented. The most appropriate method of simulation depends on a number of factors such as the system's scale (length scale or time scale) and size (number of particles), computation resources and levels of accuracy required [5, 6, 40]. For example, *ab initio* methods that are based on first principles can accurately describe simple systems in details. This is because they involve zero (or very little) approximations and guess work. This translates to explicit calculation of quantum interactions and hence tend to be extremely inefficient with respect to computation time for very large systems (large number of atoms) [5]. This, however, does not overrule their importance and use. Fundamentally, isolated model properties of systems are best calculated using this approach. In addition, systems involving small sized atoms (He and H) for which quantum effects dominate, tend to be handled by such a method.

MD is a good method that gives good dynamics of systems. In the event of a limitation of computational resource, coarse graining can be done. Course graining is not a feature that can be implemented in *ab initio* methods. The weakness of MD is that it cannot be used to describe electron transfer (as in chemical reactions) or stochastic processes. Lastly, kinetic MC is excellent for simulating stochastic processes and for events occurring at longer timescale. For instance, in deposition processes, MC can capture very well long term film evolution processes (time scale $\sim secs$) but poorly represent events occurring at the atomic time scale ($\sim fs$) such as the actual film deposition [6].

Despite these differences in simulation strategies, clear-cut exclusivity of simulation styles is not always true. In this era of parallel computation and high-speed computation, ab initio calculations are replacing some MD simulations. Such an approach is done to improve simulation accuracy. In other cases, it is possible to sacrifice dynamics of a system over the final morphology. In such a case, MD can be substituted by the kinetic MC method. In addition, mixed systems that incorporate more than one simulation technique are common. These systems either embrace some form of partnership or relay sequence in a simulation. For example vacancy creation can be a stochastic process but the material evolution be monitored by MD, or motion of lipids can be monitored by MD but chemical exchange across the lipid membrane by an *ab initio* technique [37].

The scale of modelling can vary from electronic level to the macro-scale. The average time scale and length scales also vary in the same respect. These scales are not always fixed, as there are physical and chemical effects that require more than two different scales to properly describe the mechanisms of a single system. They are called the hybrid systems. For example, reactions and dynamics of protein in a lipid membrane requires electronic model to describe chemical exchange and coarse grain models to describe the protein dynamics [12, 13].

There are many reasons that can be crafted to justify the use of computer modelling and simulations in science. Equally, there are a number of issues that also diminish the use or credibility of such an approach in science. Despite such an initial divergent introductory platform, a fairer statement would be based on the already attempted cases. It is very evident that computer simulation have given good results in studies of nanoclusters, metallic systems, material processes (such as fracture and deformation) etc. However, such results are only credible if they can be (or have been) validated by practical experiments or experimental data [5, 40].

Simulations are not foolproof tools. They are prone to errors or complications that in many cases lead to unphysical results. This unwarranted behaviour can be attributed partially or totally to the system under investigation, model and simulator (model implementer). The starting point in every simulation is that the model and algorithm used must be right. A wrong model or a bad algorithm will produce garbage results even for trivial cases [5, 40]. In contrast, a perfect model (and algorithm) that is fed in with unrealistic input will produce unphysical or experimentally divergent results i.e. garbage input produces garbage output.

With regards to the system, there can be many uncertainties about it. In many cases, this challenge arises as a result of partial or lack of understanding of parts of a physical phenomenon. Therefore, any model designed with such undercooked information will lead to an approximate. This can lead to oscillation of quality of results in the sense that the same simulation producing good results for one system while in other case, unphysical results.

In all simulation cases, calculations are involved. The challenge arises in the implementation of numerical methods. They involve approximations in calculations. This is not a bad thing if the accumulated errors are insignificant compared to the results of the simulations. In the event that only low error margins are acceptable and perhaps numerous repetitions in calculation are involved, this can be disastrous. Accumulation of errors in calculations can lead to deviations from experimental results. Such scenarios do occur irrespective of the accuracy of the formulation of model, and feed through of correct inputs [5, 40].

In simulations, physical quantities and properties are represented using variables. This form of representation allows for dynamic testing of variables and by extension physical properties. In addition, this fictitious representation can allow any system to be designed and tested. This idea of having a virtual platform makes the simulation flexible. On the counter side, this wild imagination is never true in the real world in the sense that not all cases of simulation can be turned into experiments.

Simulation algorithms are equipped with optimized tools for numerical integration, partial differential equations, exponential functions evaluation, signal analysis and other complex calculations can be invoked to solve problems that cannot solved analytically [5]. This is handy since majority of physical phenomenon involve multiple equations of such nature. In the event of that the input to such equations or parameters are dynamic, computer simulation would be more efficient. This argument is true but neither as rosy as it sounds nor necessarily true. In fact, there are physical phenomenon that are too complicated to be formulated efficiently by a theoretical model. Others cannot just be explained or modeled. Such shortfalls in models do trickle down to simulation.

In simulations, there is an apparent ability of controlling the pace at which a physical event occurs. This is because a simulation can be paused or stopped whenever convenient. The exact event at that intermediate (or final) stopping time can be visualized (graphs and images) or calculations can be made at that particular instance in time. Moreover, through the use advanced graphing and visualization tools or software (MATLAB, OVITO, etc.), 3D images can be generated and hence

physical appearance (e.g. surface morphology) can be viewed, trend and correlation analysis can be done by graphing results, images or coordinates files that can be converted into videos which may be used to provide additional explanations of the dynamic mechanisms. This property allows simulation the ability to observe dynamics of events at the atomic timescale that in experiments is impossible.

Computer simulations are safe in the sense that we deal with computer instructions via some console. The actual handling of tangible experimental objects for which some may unstable, reactive, fragile, dangerous and hazardous etc. that more or less require special environment, equipment and medium-high expertise to handle is not done in simulations. The paradox with experiments is that even simple setups are not always 100% guaranteed to give clear results. More so, such high end set of facility and personnel is very expensive. In this perspective, simulations are also cheap. On the contrary, efficient simulation setups for large systems may require advanced technology such as computation clusters is not cheap.

2.2 Simulation scale

The term scale of analysis refers to both length and time scales of the system. The definition of the length scale depends on the detail level of the system and guides the definition of the point reference particle. On the other hand, as a time scale, only the evolution of variables (or system) as a function of time is given attention. The optics of size (how big or small the particles are) is not of primary significance in time scale context [5,6].

In length scale consideration, we may describe a system as either microscopic, mesoscopic or macroscopic. For example, we may look for interactions on electronic, atomic, molecular, clusters etc. The length scale defines the laws that can be employed to study a system. For instance, macroscopic scale field variables (such as velocity, momentum and mass) are described using the continuum mechanical laws. In microscopic scale, particles are treated as discrete particles and position, momentum and system's energy are calculated using either classical (Newton's) or quantum (Schrödinger's) mechanics. It is important to note that there are systems that are best described by hybrid length scales i.e. more than one regime of the length scale is implemented [5].

In time-scale consideration, a simulation may be classified as deterministic or non-deterministic [5,6]. In the deterministic system, simulation is undertaken to capture an underlying mechanism of a physical system. Starting from some initial condition of the systems properties (momentum, positions and energies), we can predict the behaviour of the system at any point in time. The future and past configurations of system can be predicted accurately. This lies on the theoretical possibility of time forwarding or reversal.

In non-deterministic or stochastic approach, we have no means of actually predicting the past and future state of a system. The only known state is the current state. This state acts as a starting point for the next time step of simulation. However, the change of configuration is guided by a random action (e.g. generation of a random number). Stochastic models are mainly used to provide average correlations in the system's variables. Some of them are fast to implement on (very) large systems, for example kinetic MC. In addition, they can be partially implemented alongside deterministic systems whereby certain behaviour of the system is random e.g. in IBAD.

In real deposition processes (say PVD or IBAD), the sizes of the films are of the order of nano - micrometers thus requiring the microscopic length scale treatment. However, due to the large number of particles involved in a normal deposition or growth process, a classical method would best describe the system as opposed to quantum methods. This is based on the computational resource constraints [5].

In addition, there are short- and long-term effects in the deposition and post-deposition processes. Many particles move through non-linear trajectories as consequence of collision, from source to substrate's surface. It is possible to estimate or control the exact area or region for which deposition will take place on a substrate. However, the exact position (x, y, z coordinates) on the substrate for which a select atom gets deposited or bombarding particle lands, or sputtering off the surface cannot be predetermined. Therefore, such processes require a (pseudo) stochastic mediated approach. On the contrary, the motion or evolution of the atoms that are on the substrate surface can be monitored by using a deterministic approach.

2.3 Simulation and Ensemble Averages

Physical systems are composed of extremely many particles (thousands to billions of atoms or molecules) which interact through potentials (position) and collisions (velocity). These interactions are significant in the sense that it assigns different properties to every particle in the system [5,40].

The phase space is the set of momenta $\mathbf{p}$ and position coordinates $\mathbf{r}$ that can be used to describe particles in a real system or a simulation [39, 40]. At any instance in time, the set of position coordinates $\mathbf{r}^N = \mathbf{r}^N(\mathrm{t})$, for an N particle system, defines the configuration of the system. The consequent change from one configuration is called the time-step in simulation [5,39,40]. Further, if the points defined in phase space are accessible to the system and collectively defined with respect to their properties, then this collection of points can be termed as an ensemble. This implies that, ensemble properties are derived from the contribution of the individual particles [39].

The instantaneous state of each particle in phase space is called a microstate. The average contribution of all the system's microstates is called the ensemble average [39]. Ensemble averages are calculated by summing and weighing properties of individual microstates and dividing them by the total number of microstates. Properties like temperature, pressure, energy etc. measured experimentally or through a simulation are examples of ensemble averages.

To weigh microstates properly, an ensemble definition must exist. The ensemble definition in a simulation helps in management of uncertainties. In this case, it sets restrictions on the model that is being implemented. The restrictions are set with an aim of controlling variated data (i.e. inputs, outputs and parameters) or system's state. For instance, ensembles in MD are defined with respect to a set of fixed parameters such as number of particles (N), volume (V), temperature (T), Pressure (P), chemical potential (μ) or total energy (E). Combination of different fixed parameters leads to various types of ensembles such as NVE/ microcanonical, NVT/ canonical, μVT/ grand canonical and NPT/ isothermal–isobaric [5, 40].

Any system left to evolve by itself under a constant condition stabilizes to some equilibrium or stable value. Thus, after sufficiently long time, the time average observable of a system would attain the equilibrium (or stable) value, which in a hypothetical concept should be the same as the true ensemble average [5]. MD simulation measurements are rooted on this assertion. The supporting hypothesis is called the ergodic hypothesis. This hypothesis states that, if a system is allowed to evolve over a long period, it is presumed that all the accessible microstates can be visited. Hence the time averaged macrostate (thermodynamic) property or measurement (say $\langle A \rangle_{time}$) taken over long period of simulation should approach or coincide with ensemble average ($\langle A \rangle_{ensemble}$) [5, 40].

$$\langle A \rangle_{time} = \lim_{\tau \to \infty} \frac{1}{\tau} \int_{t=0}^{\tau} A(\mathbf{p}(t), \mathbf{r}(t)) dt \tag{9}$$

$$\text{i.e. } \langle A \rangle_{time} \to \langle A \rangle_{ensemble} \text{ as } t \to \infty$$

The accuracy of time-averaged values from a simulation (results) depends on the definition of system, time of simulation and statistics used in simulation. The dependence of simulation results on the system is rather trivial. The other factors are a bit abstract to conceive even for a system that is well defined.

Time averaged values may grossly differ due to violation of a system's ergodicity in the event that a smaller simulation time is used. This is because at smaller simulation times few microstates are visited. Few microstates visitation translates in bad fractional representation of a macrostate. In the context of statistics, poor statistics (low number of tries) would imply instantaneous state of the microstates are sampled. However, the microstates evolve continuously towards the equilibrium properties [5]. Hence, the properties captured by such data represent an instance of the system and not the average property of the system.

2.4 Interactions and Potentials

Every system at an elementary level can be described as made up of atoms, molecules, radicals or clusters of atoms. These particles interact in one way or another. One way of classifying interaction is by atomic bonding systems such as ionic, covalent, hydrogen, Van der Waals and metallic bonds. However, at higher levels of considerations, it is best to use atomic level potentials. Atomic potentials fundamentally underpin details that are vaguely captured by other rough representations of atoms and molecules. Despite this, there are systems which use both coarse and fine descriptions of interactions [5].

The treatment and definition of a potential in a system may be handy in classifying the level of detail of interest. For example, we may have coarse grained potentials that allow us to define a molecule or cluster as a single entity or particle, or explicitly defined potentials in which interaction level is defined per atom within a cluster or molecule. Further, the potentials may be extended to capture charge multipole and their interactions within the molecule of interest or externally with other (molecules) particles [40].

A potential system that captures a very high level of detail within the model leads towards a more accurate description of the physical system. This is because many of the particle's parameters are explicitly defined. However, on the downside, this approach becomes more and more computationally expensive as the systems grow [5]. In addition, at times it may be almost impossible or very difficult to construct an algorithm that incorporates extensively high detail level. In other cases, problems of knowledge gap may exist and hence it may not be very trivial to formulate algorithms of unknown phenomena even if we "hypothetically have infinite computational ability".

The classical potential represents interatomic potentials and adjustment terms (also called force constraints). In the event that molecules are used as base particle type, molecular force fields are used. The adjustment terms often arise due to constraints applied to a potential system or parametrized values that are enforced to the potential model to streamline it with experimental results. The classical potential can be modelled starting from a single particle term (particle under external forces), two body (also called pair potential) to many body potential such as those defining atomic clusters or metallic systems. Generally, it can be expressed as:

$$V = \sum_{i} V_1(\mathbf{r}_i) + \sum_{ij} V_2(\mathbf{r}_{ij}) + \sum_{ijk} V_3(\mathbf{r}_{ijk}) + ... + K_s \tag{10}$$

Here i, j, k ... shows the particle considered in an interaction, K_s represents constraints and V_1, V_2, V_3 corresponds to single particle term, two body term, three body respectively. The representation of V may vary from problem to problem. Our only concern is that it captures all the interactions describing the problem. Moreover, the fitting and constraining terms need not be uniform even for the same family of related problems. At times, for computational efficiency symmetry of forces (between particles i and j) is enforced i.e. $\boldsymbol{f}_{ij} = \boldsymbol{f}_{ji}$ [5].

In deposition process, the source material atoms (s), substrate atoms (R), and cross-term interactions (SR) have to be considered. This means that for a simple case of deposition only, the potential is already three atom (type) collision problem ($V = V(S, R, RS)$). However, in the case of homoepitaxial deposition, i.e. substrate atoms and source atoms are the same, the potential reduces to a two atom (type) collision problem. The potential description can still be expanded

if additional species are included into the system. For example in IBAD, the bombarding atom contribution must be accounted for in the description of the potential.

To put the case of IBAD into perspective, the film deposition or formation by a metallic species on a metallic substrate would involve at least six set of parameters to describe the problem. Assuming that we have metals x and y, and a bombarding gas g, then, the interactions is defined by the set {x-x, y-y, g-g, x-y, x-g, y-g}. However, in the special case for which source and substrate material are the of the same atom type (x = y), the collision parameters reduces to three i.e. the set {x-x, x-g, g-g} which corresponds to metal - metal, metal - gas, and gas -gas interactions.

The traditional way of addressing potentials in atomistic simulations is the use of pair potentials. These potentials are extremely good for describing gases (or gas like systems). This is because pair potential treats atoms in a system as separate entities. Such a mundane treatment cannot capture appropriately the physics of metallic systems. Therefore, the total energy, physical properties and elastic constants calculated based on pair potentials are never accurate. The fundamental aspect of metallic systems is that every bond strength is dependent on other bonds within the same system. This is in essence a many body problem [49].

The solution to this apparent gridlock is the electronic approach. The solution to many body Schrödinger equation would yield a much accurate representation of metallic system [49]. However, considering the number of particles involved, the approach would be too computationally intensive. Further, attempting to oversimplify systems results in loss of details. The biggest blow comes in handling low or nonsymmetrical systems.

The above description therefore illustrates the magnitude of a simple case of IBAD. Therefore, to address the potential problem in IBAD, different potential definitions have to be formulated to represent each section of the problem but jointly applied to give a holistic picture of the phenomenon. For example, the metal-metal interaction could be represented by quantum Sutton–Chen (QSC) potentials, while metal-gas and gas-gas by Lennard-Jones (LJ) 12–6 potential. Alternatively, metal-metal can be modelled with embedded atom method (EAM) potential [34, 48],and the rest of the interactions by Ziegler, Biersack and Littmark (ZBL) potential.

2.4.1 Embedded Atom Method

The bonding in metallic system is unique in that it is a nexus of ionic and electronic environment. This has already been seen to attract complications. However, a sufficient number of system's properties can be evaluated provided that the total energy is known [33]. Therefore, any method that is computationally efficient and can estimate accurately the total energy of a metallic system would suffice. The EAM method is one of such. This potential employs a simplified treatment of atom by avoiding the quantum mechanical solution of many electron system but simultaneously capturing the many body problem [33, 49]. For this reason, this potential has been deployed in handling metallic systems at surfaces, interfaces and bulk levels. For instance, in calculation of physical properties of metallic systems, structure and defects in metals, studying surface reconstruction and relaxation, epitaxial growth amongst others [33, 34]. Although, the EAM captures sufficient physics of metals, it is more or less of an approximate alternative to a quantum mechanical (QM) approach in metallic systems. More so, its only superiority lies on its computation efficiency.

This potential formulation is designed such that the ionic centres and the electron density are formulated as two conjoined functions. This is meant to capture the repulsive contribution and the screening of that repulsion by the electron density. The general formulation equation of an EAM potential is formulated in the basis of embedding a single atom in a metal [33,48]. The fundamental assumption is that there exists a spherical electronic density in the system. This potential can be expressed as:

$$E_T = \sum_i F_i\left(\sum_{j\neq i}\rho_j(R_{ij})\right) + 1/2\sum_i\sum_{i>j}\phi_{ij}(R_{i,j}) \tag{11}$$

Here, E_T is the total energy of the system, $F_i(\rho)$ is the embedding term that describes the background electronic (density) interaction and an embedding atom i, ρ_i is the host electron density of atom j due to the other remaining atoms in the system, and $\phi_{i,}$ is the pair potential function (inter nuclei repulsion/ also electrostatic interaction term) for the distance $R_{i,j}$ between the ith and jth atoms [48].

2.4.2 Ziegler-Biersack-Littmark potential

At high collision energies atomic nuclei approach closely to each other. The high velocities associated with such energies diminishes the capability of the electronic cloud from accommodating the temporal variations in interactions. Therefore, the system's potential can be approximated by a repulsive potential that neglects attractive force contribution. This type of interaction can be expressed using a simplified repulsive Coulomb potential.

$$V(r) = \frac{Z_i Z_j e^2}{4\pi\varepsilon_o r} \tag{12}$$

Here, Z_i, Z_j are atomic numbers of atom i and j, r is the separation distance between the two atoms, e -electron charge and ε_0 permittivity in free space.

To transition from a simple Coulomb potential to a more inclusive potential, the Ziegler-Biersack-Littmark (ZBL) potential introduced. The ZBL accommodates the effects of electron density through implementation of a screening function ϕ [34–36]. The potential between electrons and nucleus is attractive and thus acts to partially reduce (or screen) the repulsive inter-nucleus potential. This latter part assumes that the two nucleus do not overlap. This potential can be represented as:

$$V(r) = \frac{Z_i Z_j e^2}{4\pi\varepsilon_o r}\phi(r_{ij}, a)S(r_{ij}) \tag{13}$$

$$a = \frac{0.4685}{Z_i^{0.23} + Z_j^{0.23}} \qquad \text{and} \qquad \phi(x) = \sum_{i=1}^{4}\alpha_i \exp^{\beta_i x}$$

Here, α_i and β_i are numerical values that can be obtained in Ref [36], $S(r_{ij})$ is a switch function [36]. Electrostatic forces are long-range forces. For simulation purposes, a simulation box has to be sensible in size. Therefore, such considerations prompts for setting up a maximum distance for which a sensible interaction occurs. This can be interpreted as the region after which contribution from any marginal interaction has no significance effect to the simulation. Blanket truncation of the potential can lead overshooting forces (a problem that arises from attempting to obtain derivatives at discontinuities). Thus, the need to device a graceful transition between the region that interactions are accepted and the other regions for which it is ignored during simulation. This is done using a switch function $S(r_{ij})$.

2.5 Boundaries

The concept of boundaries is designed to restrict the number of particles that can be simulated in a given instance. This is because real physical systems are composed of very many particles for which not all particles can be simulated. This can be attributed to computational limitations in performing simulations.

Potential fields can be long or short range. Depending on the nature of the systems, there are instances for which non-zero interactions can be ignored. This can be in the context that their contribution have extremely little or insignificantly effect on the simulated system. In such a context, a boundary defines the limit at which an acceptable interaction exists.

A well-defined boundary condition (BC) must capture a reasonable representation of the system and its associated range of inter-particle interactions. The latter part being given more weight. Moreover, it is desirable that a BC chosen should be easy to implement and be free of artefacts associated with edge effects. Despite these desired set qualities and requirements, the choice and implementation of BCs is strongly dependent on the case under consideration.

The common boundary conditions (BCs) are open, fixed and periodic. When more than one boundary condition is concurrently implemented in the same simulation, we end up with a mixed BC. For example in adsorption and deposition studies, x and y axes may be fixed or periodic and say +/- z which is the direction in which adsorbent or evaporants travel to the surface be an open BC [47]. Mixed BCs may be prone to violation of a system's total energy conservation if they are partially constituted of an open boundary [51].

Open BC constitutes a boundary with no restrictions. In such a BC, a particle can enter or leave the simulation box depending on the dynamics of the system. This means that, energy, momentum and mass can be exchanged between the model system and the external environment [50]. This type of boundary can be used to simulate problems of natural systems such as ice formation, chemical reactions, and surface adsorption in non-equilibrium conditions [50]. However, this BC is rarely used in isolation in MD, as it can result in unusual fluctuation of particles [5]. The worst case scenario is where the system may outgrow the projected simulation capacity, or all the particles may exit the system.

Fixed boundaries constitute a BC in which particle subtraction from (or addition to) the simulation volume is prohibited. The boundary atoms are cleverly excluded from the simulation system e.g. the velocities of the atoms are zeroed at the boundary and atom positions fixed [38]. An alternative implementation may involve use of a sacrificial or buffer region between the system and boundary to accommodate any unrealistic effects that may attributed to such arrangement. This type of boundary condition has been successfully used in controlled simulation of calcium oxalate crystal growth [47]. Fixed BC is not efficient in evaluating thermodynamic properties. It generates an error $\sim \mathrm{N}^{1/3}$, where N is the number of particles simulated [51].

Periodic boundary condition (PBC) is used to model an infinite system using a finite simulation cell. This is achieved by having a fixed number of particles within a simulation cell and making periodic images of the simulation box. A particle exiting from one end of the simulation box is interpreted as the same particle entering the simulation box from the opposite direction. In this BC, there is always a cutoff range of interaction. This cutoff is set to prevent a particle from interacting by its own image [5, 50, 51]. This type of boundary provides the fastest convergence in calculation of average potential energy and pressure as a function of system size growth [51]

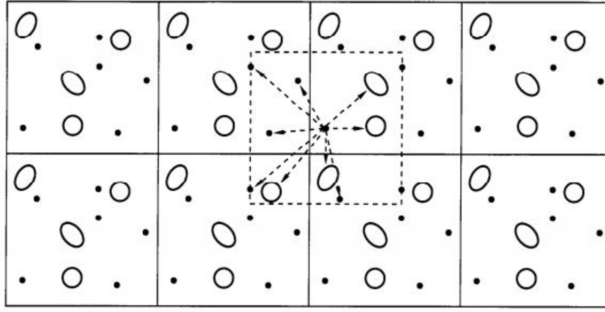

Figure 15: Selection of primitive cell and its images in a periodic boundary condition.

PBC is superior to a number of other boundary conditions in simulating homogeneous bulk-like systems. It is an elegant method in addressing the continuity of interactions (forces) along the edges. More so, the freedom of selection of the origin is another desirable factor [5, 38]. However, this type of boundary condition is ineffective in describing systems that are dominated by long-range forces [5,38]. in such a case, limiting system size becomes problematic. Moreover, simulation of symmetry breaking transitions are poorly captured by this system. The biggest weakness is the simulation anomalous size effects of liquid. PBC tends to interfere with the structure of such liquids and hence inaccurate thermodynamic properties result [43, 44]. Lastly, it has a weakness of addressing growing systems size. This is because the box size is predefined and number of particles fixed.

2.6 Temperature Control

Real systems are never perfect in the sense that they can never be handled in isolation of the environment. Experiments show that there is always leakage (of energy, temperature etc.) to the external environment. In other words, provided there is an accessible gradient of any physical quantity, there will be influence by the external environment. To accommodate or regulate the effects of the environment, artificial measures are introduced in the experiment. For example, thermostats, barostats, heat baths are incorporated in the system to regulate system's properties such as temperature and pressure. To produce similar effects in a simulation, an ensemble that reflects laboratory conditions such as NVT or NPT ensemble [52] is used in (sampling) a simulation.

The instantaneous temperature $T(t)$ of microstates can be correlated to the kinetic energy through the particle momentum $\mathbf{P}$. If the particles are identical, then we can simply talk of the particle velocity $\mathbf{v}$. However, what is measured is the time average temperature T of all the microstates, i.e. average system's temperature. This quantity depends on the number of particles as well the constraints applied to the system i.e. degree of freedom of the system N [52]. For a simple system without constraints, T can be expressed as:

$$\sum_i \frac{\mathbf{p}_i^2}{2m_i} = \frac{3}{2} N k_b T \tag{14}$$

$$T = \frac{1}{3Nk_b} \sum_i \frac{\mathbf{p}_i^2}{m_i} \tag{15}$$

This relationship between T and $\mathbf{v}$ suggest that the temperature of a system under NVT simulation can simply be controlled through velocity rescaling.

If we define a scaling parameter λ, then, the change in temperature at any instance can be defined as:

$$\Delta T = (\lambda^2 - 1)T(t) \text{ where } \lambda = \sqrt{\frac{T}{T(t)}} \tag{16}$$

This simple velocity scaling is what is implemented in Berendsen thermostat where the temperature of a system is connected to a heat bath of temperature T_0 [52]. The successive changes in temperature as function of time step (dt) adopts an overall exponential relaxation towards the desired temperature. If we define a coupling parameter τ between our system and the heat bath, then:

$$\frac{dT}{dt} = \frac{T_0 - T}{\tau} \tag{17}$$

A quick assessment of Equation 17 shows that in the limit $\tau \to \infty$, Berendsen thermostat switches off. The limit $\tau \to 0$ is a case of having extremely low temperature fluctuations, while $\tau =$ dt, the thermostat performs linear temperature control. Typical values for $\tau \sim 0.1$ ps in MD [52].

Using an optimal range for a sensible τ, Berendsen thermostat relaxes very fast and shows very little fluctuation. This makes it an efficient means of reaching a target temperature as implemented in many equilibration processes. However, in NVT (canonical) ensemble that is commonly adopted for sampling in MD simulations, the simple velocity rescaling becomes inappropriate. Another disadvantage is that the quick relaxation has potential of removing a large quantity heat from a system at every time step. Such a behaviour is a poor representation of real physical systems.

2.7 Integrators

The Velocity Verlet algorithm is a popular integration algorithm in MD. It is fast, accurate for elongated time steps and requires little memory to implement. This makes it a suitable method for handling large systems. The algorithm's approach to short-term energy conservation is acceptable [5].

This algorithm computes positions, velocities and acceleration at the same time step without necessarily compromising on the acceptable levels of accuracy. The equation representing the position and the velocities can be written as:

$$\boldsymbol{r}(t + \Delta t) = \boldsymbol{r}(t) + \Delta t \boldsymbol{v} + \frac{1}{2}\Delta t^2 \boldsymbol{a}(t) \tag{18}$$

$$\boldsymbol{v}(t + \Delta t) = \boldsymbol{v}(t) + \frac{1}{2}\Delta t[\boldsymbol{a}(t) + \boldsymbol{a}(t + \Delta t)] \tag{19}$$

The Velocity-Verlet algorithm is not flawless. It may exhibit long-term energy drift. Just like any other integration algorithm, it may suffer from floating point truncation errors in computing time reversal processes. The other variant version of the Verlet algorithm is the Leapfrog algorithm. It involves the calculations of velocities explicitly. However, in the implementation of the algorithm, velocities are calculated at half integer time steps while positions at full integer steps. The algorithm can be expressed as follows:

$$\boldsymbol{v}(t + \frac{1}{2}\Delta t) = \boldsymbol{v}(t - \frac{1}{2}\Delta t) + \frac{\boldsymbol{F}(t)}{m}\Delta t \tag{20}$$

$$\boldsymbol{r}(t + \Delta t) = \boldsymbol{r}(t) + \boldsymbol{v}(t + \frac{1}{2}\Delta t)\Delta t \tag{21}$$

The algorithm increases the accuracy of integration by minimizing the round off error.

2.8 Molecular Dynamics Simulation Algorithm

Molecular Dynamics (MD) studies equilibrium behaviour and transport of systems based on classical description of atoms (or molecules). In its pure state, it strictly implements Newton's laws of motion to solve for trajectories, energies and other physical properties of atomic systems [5, 6].

MD treats a system from the molecular level, and it is a bottom up approach method of modelling. It is most applicable at scales for which the discrete nature of molecules is significant. The main advantage of using MD simulation is due to its simplicity and relatively reasonable system size that it can handle. Moreover, it can easily allow for coarse grain definition of simulation particle, and thus accomodating larger system sizes than convectional definition of particle (atoms or small molecules) [6].

Newtonian mechanics requires less intensive and abstract background physics in comparison to quantum mechanics. In many instances simple theoretical treatment such as numerical integration and basic physics is required to understand the mechanism. This is a major advantage with respect to understanding the mechanism behind MD. However, post processing techniques and data interpretation in MD, just like other methods, may require additional statistical knowledge and advanced physics to accomplish.

In MD, particle interaction for any given system is defined purely on position dependent potentials U. If assignment of masses m to particles within a closed system (i.e. total energy E and momentum $\mathbf{P}$ are conserved) is adopted, then we can use the definition derivative of scalar field to define inter-particles' forces $\mathbf{F}$. This can be expressed as $\mathbf{F} = -\nabla U$. Then, by invoking Newton's second law of motion ($\mathbf{F} = m\mathbf{a}$), acceleration $\mathbf{a}$ can be calculated from the forces. The velocity $\mathbf{v}$ of the system and new positions $\mathbf{r}$ can be calculated using a suitable time integrator algorithm such as Velocity-Verlet or Leap-frog algorithm. The general MD algorithm takes the form in Figure 16. There can be deviations in the exact implementation case wise.

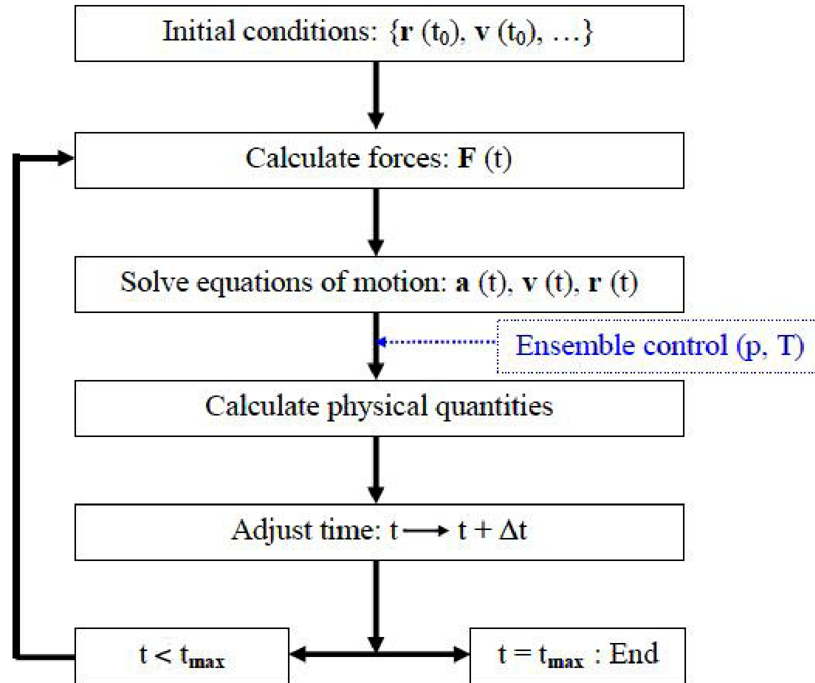

Figure 16: Molecular Dynamics Algorithm

This simulation method is computationally intensive as the system size grows. Thus has limits to the system size it can handle i.e. the method cannot work for infinitely large systems of particles. This is a downside of MD. The common alternative approach to handle larger systems is to do coarse graining approach. Here, the definition of particle is elevated from single atoms to group of atoms (molecules, clusters etc). The course graining approach is prone to lose of details and hence has higher chance of poorly representing a physical phenomenon. However, with a carefully chosen sample size, it is possible to get meaningful results.

Another downside that is inherent with this modelling method approach is that it is a deterministic approach. Thus, any physical system that exhibits stochastic tendencies is not compatible with this model. However, if only a section of the entire simulation is random, MD can find use. Such as a specific case requires a calculated implementation of a simulation algorithm. For instance, separate handling of portions of physical phenomenon that are stochastic in nature are catered for using some independent routine (code or program) and that is called within the MD routine.

2.9 Growth simulations in MD

The ultimate goal of a growth simulation is to develop a model that captures specific issues within a growth process. For a start, the model should clearly demonstrate the correlation between the simulation parameters and the final film morphology. This is important especially where film texture is of great significance. For example, in IBAD, it is possible to attempt to correlate the growth mode that results from controlling bombarding ion fluence, or the effect of bombardment energy on the texture or roughness of resulting film for a fixed ion fluence.

There is never a 100% real crystalline surface. Real solids that are termed as "crystalline", always have few areas or regions marked with minor crystal defects or deviant crystal orientation. More so, new and clean surface evolution such as surface layer rearrangement (relaxation and reconstructions) or contamination always influence the growth of the film layer. For example, in PVD, adatoms or contaminant atoms can act as nucleation sites or even as shadowing sites of film especially if low energies are used. Therefore, a simulation algorithm must address the concepts of defects in the surface and interfaces region. The interface definition is not restricted to film-substrate boundary but also for regions with different crystal order appear, and crystalline-amorphous boundary of the film.

In the event that high energy particles are used in MD, depositing or bombarding atoms have sufficient energy to diffuse over the surface or even cause surface migration by transfer of momentum to substrate atoms. These atoms have the potential of getting to the most favourable sites. In most cases, voids are likely to be filled first. This ensures that problems like formation of voids and subsurface vacancies that have a possibility of occurrence can be neglected in the formulation of the algorithm. However, the interfacial boundary has to be included in the study in order to observe the dynamics surrounding (conformal) coverage deposition (in PVD or IBAD).

The effects of stress on films can be detrimental. Stress in films can occur as early as the deposition stage or very late stages of usage of a final product. During the deposition process, the intrinsic stress ought to be investigated and possibly mitigated. Investigation can intended to establish the correlation between deposition variables (such as energy and ion fluence in IBAD process) and stress evolution in thin film. In addition, it may be beneficial to attempt to correlate other processes such as formation of defects and grain growth in relation to the stress evolution in film.

2.10 Thesis simulations

This thesis attempts to look at IBAD process under various conditions and the effect of those conditions on surface roughening and film stress. The initial case is reduced to purely a PVD case. This is because the ion source is switched off and deposition of Cu on Cu substrate using different deposition energies (i.e. E_{Cu} = 0.3, 1, 3, 10 and 30 eV). In the second case, Cu deposition energy is fixed at 1 eV (E_{Cu} = 1 eV) and then different ion bombardment energies (E_{Ar} = 1, 2, 5, 10, 20, 30 and 50 eV) are tested. In the final case, the bombardment and deposition energies are fixed at E_{Ar} = 30 eV and E_{Cu} = 1 eV respectively. The control parameter in this latter case is the Ar fluence. Ar fluence of 0.2, 0.5, and 0.8 ions/nm^2 are tested.

The entire simulation runs were done using Parallel Cascade (PARCAS) molecular dynamics simulation code. In the simulation, a minimum of 4000 runs for each case is done. The 4000 runs is the same as 4000 deposition cycles in PVD but in IBAD it is includes the bombardment cycles as well. In most cases, this successfully grows over 9 layers but in some cases extra runs are to be carried to achieve this. Since every simulation takes approximately 10 hours on 4-core processor computer, some of the simulations were done on Alcyone computational cluster of the University of Helsinki. The estimated time for completion is less than 2 hours on 12 cores.

In this setup, we have single gun (that acts as both ion and atom source) that is fixed above a copper substrate. The position of the gun is (x, y, z) = (0, 0, 50). The ion source shoots either an argon ion or copper atom at any instance. The particle types are already predefined (Ar or Cu species) but the frequency of the "type" that exits the source (gun) is determined by set probability i.e. the recoil atom is determined by some set fluence. This fluence determines the ratio of bombardment to deposition rates. For instance, when the fluence is set to zero, the deposition rate is 100%. This means that every simulation cycle is a deposition cycle. Therefore, at zero ion fluence, can be translated as Cu on Cu PVD process.

In real PVD deposition takes place within a defined area. The order in which successive incident source material land on the substrate is random. The actual bombardment assumes the fashion of rainfall on to the ground. The only difference is that we can control the frequency of the ion shower by tuning the ion fluence. Since the incoming source material and ions come from a fixed point, there has to be different alternative method to induce the random substrate impingement. In this respect, the box is shifted randomly. To have an imagination of this implementation is to fix an observer on the substrate. Since the observer moves with the substrate, the apparent observation from the substrate as reference frame will be a mobile (ion or atom) source.

In the context of this simulation, the concept of randomly shifting the simulation box is a virtual representation of the actual process. The position of the box is fixed as far as the arrangement of the simulation is concerned. What is actually called random motion of box is rather collective motion of all atoms in the box using some random distance. In other words, all atoms making up the immediate substrate shift with the same magnitude (x & y coordinates) on substrate at the same time. The overflow on the edge of box by atoms is accommodated by using periodic boundary condition. The same effect would be achieved if we held the atoms constant, shifted the box randomly (and enforced periodicity) along x-y plane.

In this arrangement, a linear trajectory of propagation only one species is produced at a time. This eliminates interparticle collisions before arrival at the substrate that may modify the incident particles' momenta. Moreover, only one species reaches the substrate at any instance. This is a simplification of the exact IBAD.

In real IBAD, the source material production and ion generation in processes are independent. This implies that two different particle species can be produced simultaneously. Moreover, more than two Cu atoms or Ar ions can be produced, and Cu species and Ar species may impinge on the surface simultaneously. Further implication of such arrangement, it prohibits substrate site competitive deposition. This means that whatever happens to single surface atom due to double contribution of the bombarding ion and depositing atom is not well represented in this arrangement. This, however, does not downplay the control the frequency for which bombardment can be controlled.

The random nature of the interparticle collision along the trajectory is partially captured in this simulation indirectly. This is done by setting the angular dependencies of source particles (say, Ar ions) randomly. This is a direct imagination of the final part of trajectory of an incident particle before landing on the substrate. In addition, random shifting of the simulation box ensures that the deposition location on the substrate by the incoming particles is never predetermined. The only downside of this arrangement is that in collisions momentum modification by collisions is neglected.

The potential system employed was the EAM for Cu-Cu interaction, while for Ar-Ar and Ar-Cu it was set to ZBL repulsive potential. This was done to ensure that no Ar gets adsorded on the metallic film or substrate but rather acts as a momentum carrier to the surface atoms i.e. like a hammer driving a nail in wood. The potential files were supplied as part of the input files.

The full set of virials W consisting of a nine component tensor was generated by PARCAS. The indifference to symmetry of the stress tensor was not of great concern, as the most important values were those that lied along the diagonal axis (W_{ij} where $i = j$) of this tensor. In every simulation cycle, the diagonal terms of the tensor were copied (alongside the atomic coordinates) to some final position file. The other six components of that tensor are ignored to reduce the size of the final file, and also for the reason that they are not used anywhere in the final analysis. However, the scientific argument is because the film thickness is much less than the substrate thickness. In such a case, the biaxial stress asserted on substrate is assumed isotropic and relatively homogeneous. Thus, the off diagonal terms of stress σ_{ij} where $i \neq j$ can be assumed to be zero. An elongated proof can be deduced through derivation of Stoney's formula [4, 54].

The simulation execution was aided by bash script and Python script. The design of the system was such that the simulation could be stopped and restarted at any given point with little modification. This was achieved by ensuring that each input file is stored with a numerical value attached to that simulation, and output files were stored in the same fashion. The final atomic positions were copied from md.movie file to an .xyz file. Each final .xyz file was enumerated and stored separately. The execution was aided by bash script and Python script. The motivation behind this was that the visualization tool (OVITO) had the capability of aggregating trajectory files using a wild card pattern [55].

The PARCAS units for length is the Angstrom (1 Å $= 10^{-10}$ m), time is measured in femtoseconds (1 fs $= 10^{-15}$ s) and energy is measured in electron volt (1 eV $= 1.602 * 10^{-19}$ J). The other crucial units are internally derived in PARCAS. The masses m_i, though entered in their actual correct atomic mass units, are transformed to unity (m = 1). This is done by ensuring that the atom type's velocity is dependent on mass. This is obtained transforming the kinetic energy such that $E = v^2/2$ where $\mathbf{v} = \mathbf{v}(m)$ measured in m/s, and E is the energy in eV.

A summary of the parameters used in running the simulation included a simulation cell of (in Åunits) (x,y,z) = (36.3584, 29.08512, 29.08512) with 10, 8, 8 cells in the x, y & z respectively. The time step used was 0.05 in internal units, the atom types used were 2 (Ar of mass 28.086 au and Cu of mass 63.54 au). The substrate at time zero for all simulations had 4096 atoms. The interaction was declared as pair for non-metallic pairs while Cu-Cu was set to EAM. The boundary condition was set to (x,y,z)= (1,1,0) where 1 represent periodic boundary condition. Temperature control was set to linear up to a final temperature of 300 K. For the purpose of generating the full set of virials, moviemode 15 was used.

Post deposition processing was done in Python. Majorly plots were exclusively done in Python. The other intermediate processes, though done through a Python script, were not exclusively Python's. Python through the package "os" can execute Linux commands. Therefore, a cocktail of bash, awk, OVITO and Python procedures were all used for intermediate processing. However, 3D visualisation of the actual deposition process and image caption of stages of deposition was exclusively handled using OVITO.

2.11 Surface roughness and stress analysis

The imagination of a perfect flat surface (molecular level flatness) does not exist in real solid materials [56]. Surface texture is the deviation of the nominal surface. It is more of a topographical map of a solid. Depending on the magnification level or instrumental sensitivity, texture can be roughness (nano- and micro-roughness), waviness (macro-roughness) or even surface flaws [56].

At the atomic level, roughness is just the measure of micro-maxima and micro-minima on the surface relative to some average surface height [56]. Surface roughness can be estimated using statistical quantities inclusive of center-line average, arithmetic average, standard deviation or variance, root mean square and extreme-value height descriptors [56, 57]. In this context, the square mean fluctuation of the film height also called the statistical variance has been used. If we define mean film surface height as $\bar{z}(i,t)$, then, the variance or roughness (w(L,t)) is calculated as:

$$\bar{z}(t) = \frac{1}{L^d}\sum_{i}^{L^d} z(i,t) \tag{22}$$

$$w(L,t) = \frac{1}{L^d}\sum_{i}^{L^d} \left[z(i,t) - \bar{z}(i,t)\right]^2$$

Here L^d represents the linear size of the network (L) in the correct dimensionality (d). In the terms of deposition, L represents the number of atoms in the x and y axes of the surface ($d = 2$). The roughness is measured in every time step (simulation frame) to capture the instantaneous change of the surface structure as the deposition changes. This is done for obvious reasons that a surface atom can be converted into a bulk atom if more atomic layers pile up during deposition.

The stress experienced by the film during deposition can be estimated by using Stoneys equation:

$$\sigma = \frac{E_s t_s^2}{6(1-\nu_s)}\frac{\kappa}{t_f} \tag{23}$$

Where the substrate's parameters E_s, ν_s, and t_s corresponds to the Young's modulus, Poisson's ratio and thickness respectively. The variable t_f is the instantaneous measured thickness of the film. The parameter κ measures surface curvature. If we impose a periodic boundary condition that the bending at the edges is always wrapped on the opposite side of the substrate's block, then, it can be assume that the curvature is relatively constant. In addition, if further restriction is imposed that $\nu_s = 0$, then the reduced Stoney's equation can be used to estimate stress evolution as function of thickness [58]. This relation shows that the inverse relationship between film thickness and stress.

The stress values are indirectly obtained from the virial output of PARCAS. The concept of the virial system is derived from pressure calculation in MD. To illustrate this, an arbitrary system containing N particles interacting through a potential U, confined in a simulation volume V and temperature T is defined. The pressure P of such a system can be calculated as:

$$P = \frac{Nk_bT}{V} + \frac{\langle W \rangle}{3V} \tag{24}$$

Here, W is the internal virial term that represents the contributions of the interaction potential to the pressure. Since forces $\mathbf{F}$ acting between atoms at instantaneous positions $\mathbf{r}$ can be obtained by getting derivatives of the potential U, W can be expressed as $W(\mathbf{r}^N) = \sum_i^N \mathbf{r}_i \cdot \mathbf{F}_i$. The various forms of W for infinite periodic systems or finite non-periodic system are provided for in Ref [60]. The virials W_{ii} can be computed directly from PARCAS in units eV. To define stress, the viral is defined with respect to the atom position (film height z above the substrate's surface). Since the atoms are identical, atomic area/volume are scaling effects on the forces computed from the virials.

To perform any form of analysis, only the surface atoms have to be considered. Therefore, there is a need to extract the surface atoms from the bulk substrate. There are a number of methods that could be used for example centrosymmetry deviation, bond orientation order and common neighbour analysis [59]. In this setup, a simple coordination number analysis of FCC Cu has been used. The assumption is that all bulk atoms have coordination number of 12. Any deviation, assuming that there are no crystal defects, suggests that the atom in question is a surface atom. Further, a bias dynamic thickness is set up such that the edge surface atoms of the bulk in the final profile are excluded from the extraction process. This also accommodates the expanded definition of substrate in the sense that after many (say fourth/ fifth) complete monolayers have formed, the first monolayer is no longer part of the surface. Therefore, we have to redefine the surface. This is the idea behind dynamic thickness

There are two ways of extracting surface atoms through the coordination number. The primary one involves writing a script that calculates absolute spacing around a selected atom i with its neighbours and counting that atoms whose distance (for Cu) to be approximately 3.08 Åt́o be members of the first coordination of that atom. The cutoff distances could be derived through lattice spacing and atomic radii of atom (in this case, copper). A shorter means would be to get that value from OVITO for it has a list of cutoff of nearest neighbours for common elements [55]. The dynamic thickness is also calculated in the script for every time step. In this implementation, since every final event of every time frame is stored separately (in numbered .xyz file), this method is most efficient if done in a parallel manner.

The other option is to use OVITO. In OVITO's approach, the modification have to be applied on a (series of) frame(s). The implementation is in this order: Expression select with options Boolean expression (Position.Z>29.0 && coordination<12), Coordination Analysis (for function Coordination), Invert selection, Delete selected particles and Slice. The resulting output is exported in .xyz file format to print out the surface atom file. The fields on the output file e.g x, y, z, wxx, wyy e.t.c. can be selected by user. An additional script can be implemented to correct height (Position.Z) predefined in the Boolean expression i.e. dynamic thickness bias.

3 Results

The initial surface used in all simulations is a typical clean surface. This equilibrium starting surface atoms consists of three level of atoms, partly of the complete sky blue monolayer, the incomplete green layer and the two yellow atoms of the third level layer. In Figure 17, all the underneath initial substrate's atoms have been sliced out of the images. The final surface shows a well layered profile. However, the excellent layering shown in this case is due to saturation in simulation. Therefore, for the purpose of analysis, the subsequent analysis would be focused at an earlier time before the saturation regime is reached.

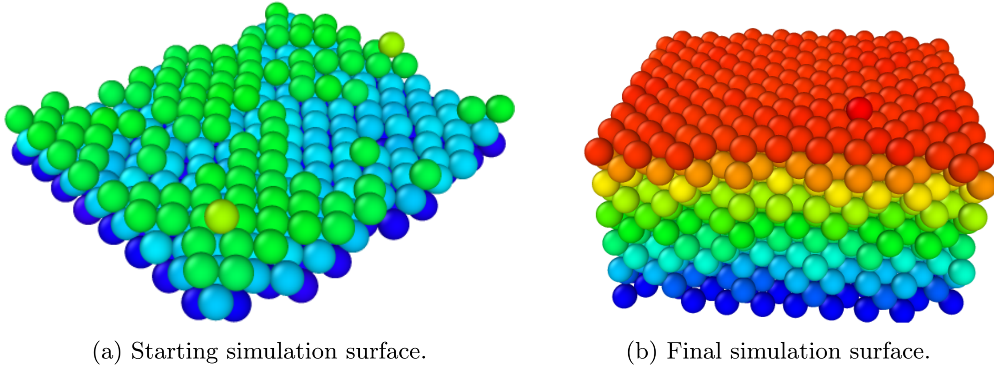

(a) Starting simulation surface. (b) Final simulation surface.

Figure 17: Starting and saturation film profile

The set-up allows a maximum number of 9 monolayers to be deposited or height equivalent to 9 perfect monolayers. After this limit has been reached, atomic deposition is capped. Any development at heights higher than 9th atomic layer are partially influenced by the effects of that height ceiling. This critical level or height will be referred as saturation point and the atomic layer associated with the saturation height will be called saturation layer. For short notation, they will simply be referred as saturation. To have independent analysis of the system's short falls, analysis is restricted to a limit lower than saturation layer.

The time taken to reach saturation is fastest in all cases for which no bombardment is applied. It is reached earlier in the case of PVD at $\sim$ 1900 cycles in comparison to IBAD at $\sim$ 3500 cycles. This is attributed for two possible reasons. The setup is such that the ion gun releases only one ionic species at a time. This means that in PVD (no bombardment), every simulation step is a deposition process. In the case of IBAD, the fluence of bombarding ion (Ar ions) dictates the deposition cycle. For instance on an equal deposition and bombardment cycle (50% Ar ion fluence), translates on an average to 50% less frequency of deposition rate compared to PVD. In addition, the motivation behind the simulation endeavour is to have net deposition of copper, and hence a successful deposition translates to addition of three Cu atoms. Therefore, the greater the frequency of deposition, the faster the saturation is reached. The second reason may be attributed to a high probability of net sputtering event, for some cycles, taking place in the case of IBAD.

In pure PVD, roughening decreases with increasing particle energy. At 30 eV, growth is layer-by-layer as seen in the nearly uniform variance profile. This assumes that artefacts around the saturation region are ignored from the analysis. At 30 eV, an adatom is presumed to be having sufficient energy for both terrace diffusion and energy to overcome the ES-barrier. The adatom's diffusion length is also likely to be long enough to give an adatom the flexibility of locating the most favourable surface site during the deposition i.e. efficient intralayer and interlayer transport.

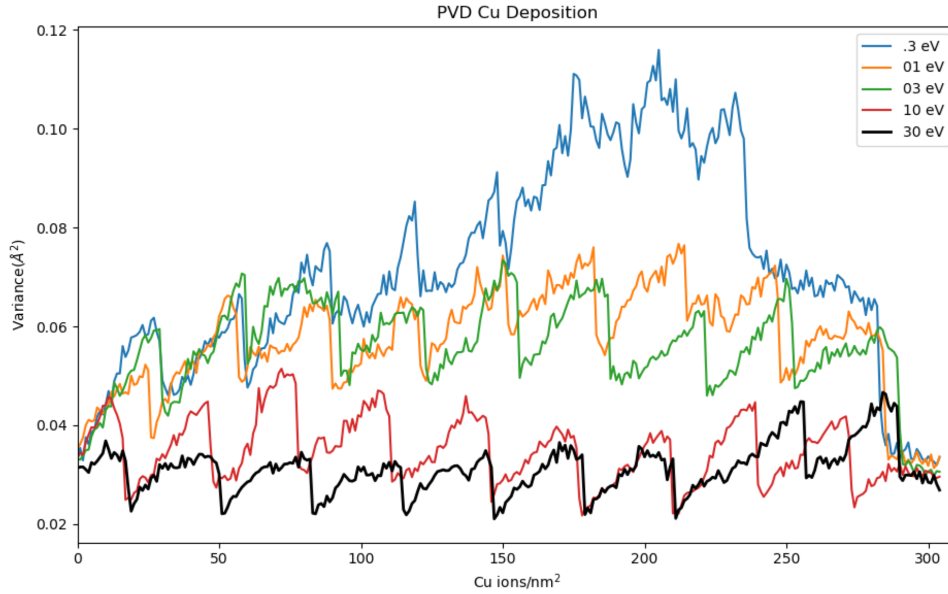

Figure 18: PVD Surface roughness profile

In contrast, at the lowest energy 0.3 eV, roughness is most pronounced. This is because at deposition energies of this magnitude, the incoming atoms in a sense lack sufficient energy to overcome the initial energy barrier i.e. adatom diffusion is frozen. This literally implies that a surface adatom is immobile at the point of contact. This favours stacking up of atoms causing poor layer uniformity. This is in the sense that a new level (representing a potential position of a new layer) is formed before the previous layer is completed. This is what causes subsequent rise in the average height of surface atoms.

In pictorial sense, using time step 1000 as a model, shows the same features as those in the variance plot. The lower energies are characterized by direct vertical arrangement of atoms with regions that resemble inverted frusta, pyramids, ridges and poorly conditioned terraces. Five successive layers are incomplete in Figure 19a. Surface coverage improves at 3 eV whereby extreme step heights are diminished. This condition is almost non-existent in the case of 30 eV (Figure 19c), with the assumption of the few adatoms (brown atoms). The few pockets seen on the topmost layer are either for purpose of equilibrium structure and insufficient number of adatoms to cover completely the top most monolayer. This latter deduction is a direct inductive reasoning from the initial equilibrium starting structure.

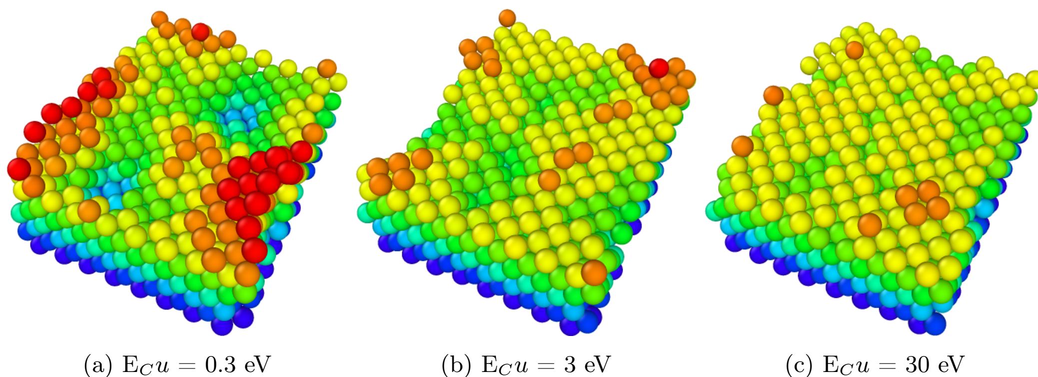

(a) $E_Cu = 0.3$ eV (b) $E_Cu = 3$ eV (c) $E_Cu = 30$ eV

Figure 19: Surface images for PVD after 1000 impacts

Despite the rugged nature of the surface profile at 0.3 eV, there exists complete layers. The atomic layers close to original substrate surface are indeed complete. This suggests that the stacking nature of atoms is dominant but not definite. There are forces such as those originating from surface energy or nucleation process are still in play. The impact is minimal but not zero. The only definite aspect of deposition at this energy is that the deposited atom does not primarily occupy the most preferential site unless it landed on the preferential site on impact.

In the case of IBAD, at a constant Cu deposition energy ($E_{Cu} = 1$ eV) and varied Ar bombardment energies (which will be denoted as E_{Ar}), a similar trend to that PVD ensues. The degree of roughness measured as variance is seen to smooth out at high bombardment energies. The lowest variation is witnessed at $E_{Ar} = 50$ eV, whilst other energies show outright roughening.

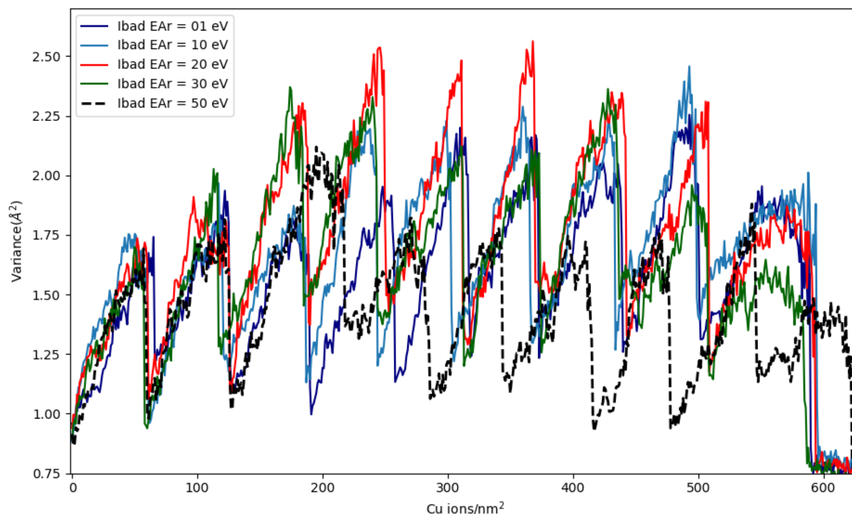

Figure 20: IBAD surface profile

The general line of reasoning is that at lower particle energies, efficient interlayer and intralayer diffusion is limited. Hence, a more favourable stacking of atoms i.e. island like growth. The only difference with lower energy PVD is that there are no empty deposition cycles. However, at high energies, there is a reasonable chance that both momentum transfer (source of diffusion energy) and sputtering taking place. Weakly bound atoms such as isolated surface adatoms, atoms at atomic projections and atoms at points of high curvature are likely to be sputtered out on impact. In the event that no sputtering takes place, an invigorated surface atom is likely migrate to a more stable or favourable surface site. Therefore, at higher energies, the probability of island growth or formation is miniaturized by both diffusion and sputtering. This explains the observation of improved layer-by layer growth at high bombardment energy ($E_{Ar} = 30$ & 50 eV).

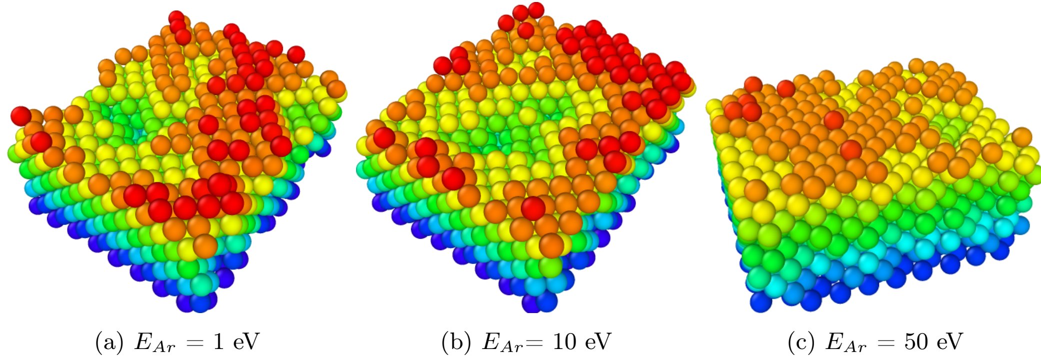

(a) E_{Ar} = 1 eV (b) E_{Ar}= 10 eV (c) E_{Ar} = 50 eV

Figure 21: Surface images for IBAD at 2300 cycles

3.1 Effect of energy on layer growth

At a fixed bombardment rate of 50% ion fluence, the improved layer by layer growth in IBAD by increasing bombardment energy is not good enough. In comparison with the best layered PVD profile at E_{Cu} = 30 eV, depicts PVD as superior to the best of IBAD. On a qualitative scale, if the the eighth layer of incomplete atoms is truncated, IBAD produces a relatively nicely layered profile at E_{Ar} = 50 eV. However, even with such treatment, there are aspects of perfect surface abnormalities (vacancies) that are a present. Therefore, PVD it will used as a reference for layer-by-layer growth.

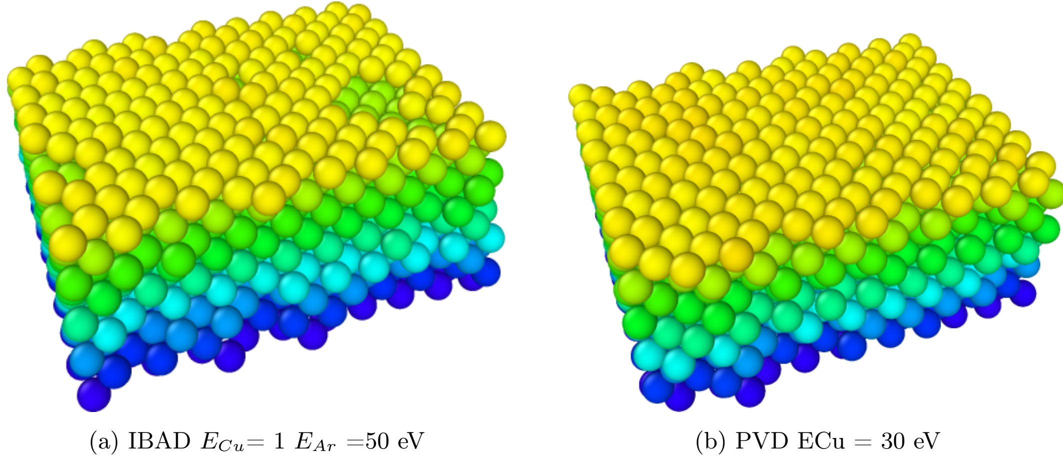

(a) IBAD E_{Cu}= 1 E_{Ar} =50 eV (b) PVD ECu = 30 eV

Figure 22: Layer by layer growth comparison between PVD and IBAD at high energy deposition

A quick comparison between growth modes having PVD at 30 eV as the baseline reveals that IBAD at E_{Ar} = 50 eV bombardment energy favours growth closest to the perfect layer by layer growth. The variance plot shows a better horizontal stability for the case of E_{Ar} = 50 eV and seemingly frustrated stability for E_{Ar} = 30 eV.

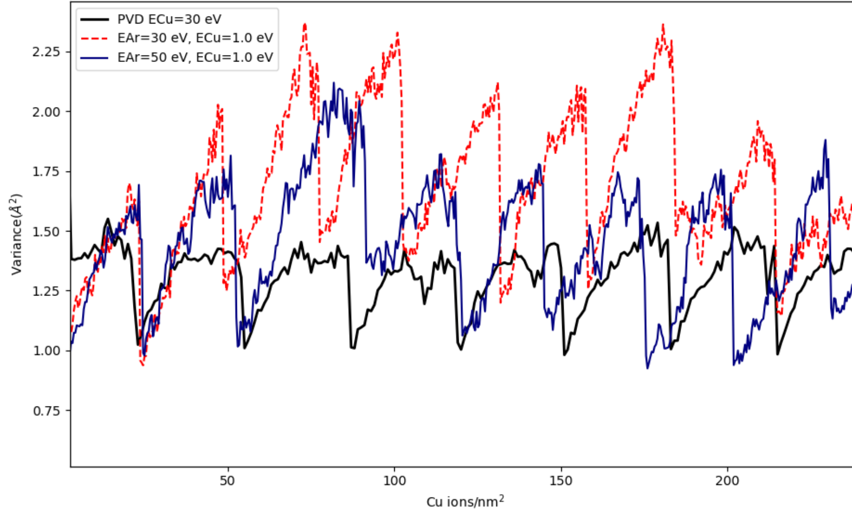

Figure 23: Growth mode variance plots

The baseline established by PVD raises a basic question as to why very high energy ($E_{Ar} = 50$ eV) is required to get the layer by layer growth and not the same order of energy magnitude of ~ 30 eV in PVD as demonstrated in Figure 22. To address this issue enough, it is important to start by explaining a few guidelines that are required for analysis. The layer stacking rates for PVD and IBAD are different. Therefore, as opposed to focusing on the times to give rise to a certain layer or thickness, the absolute number of layers is compared here. The first eight stacked layers collective having a thickness of $\sim$ 14.5 Åḿeasured above the substrate surface are used as the standard of comparison. To make visualization easier, the eighth layer atoms are colour coded as brown. Moreover, the contribution of the deposition energy $E_{Cu} = 1$ eV in IBAD is given least consideration. The main reason is that high bombardment energy ($E_{Ar} \gg E_{Cu} = 1$ eV), bombardment dictates the nature of surface processes. To start the analysis, the visual evidence is presented before presenting other technical information.

The pictorial evidence in Figure 24 shows that ion bombardment at $E_{Ar} = 30$ eV, the layering is poorly completed. Vertical growth (island growth) occurs at a much faster rate than layer-by-layer growth. This spasmodic growth progression is seen to affect the last 3 layers below the topmost layers. In comparison, bombardment at $E_{Ar} = 50$ eV yields a much better layering. Only the layer beneath the surface has few abnormalities. The sporadic island growth manifestation at $E_{Ar} = 30$ eV whereby the 9th layer grows in the form of an island at the expense of the levels beneath is not evident at $E_{Ar} = 50$ eV.

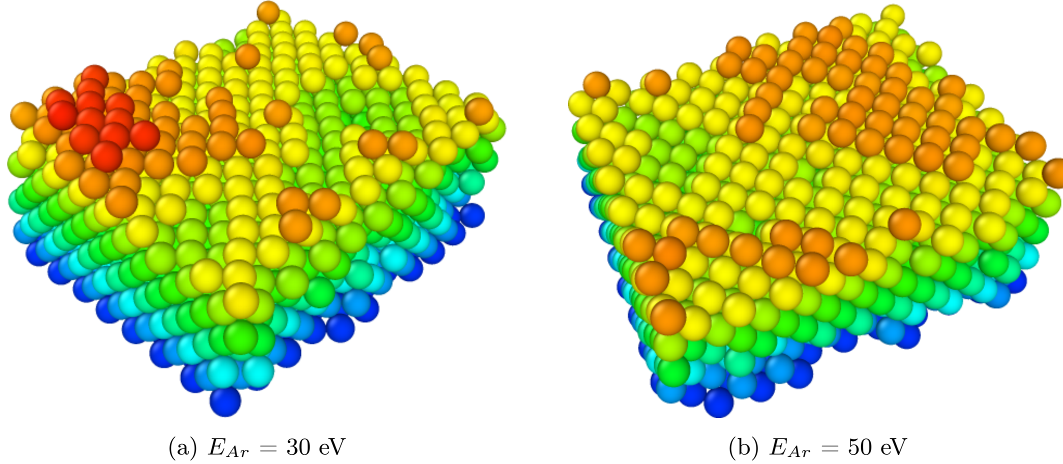

(a) E_{Ar} = 30 eV (b) E_{Ar} = 50 eV

Figure 24: IBAD images for high Ar bombard energy at constant Cu (E_{Cu} = 1 eV)

For a start, a comparison between the best layered PVD profile (E_{Cu} = 30 eV) against an equivalent energy IBAD process (E_{Cu} =1 eV & E_{Ar} = 30 eV) is assessed. In PVD, all atoms arriving on the surface have the same amount of energy. In the case of IBAD, the amount of energy transferred by the incident Ar ion depends on the angle of impact on surface atom, the number of atoms collided with at impact and energy cascade pattern of surface atoms. This is simply to say that in some instances, the amount of energy transferred by an incident Ar ion collision is a one sided and short-tailed distribution with a peak at 30 eV. Therefore, whilst all the atoms in PVD behave nearly in the same way, in IBAD a range of behaviour is to be expected. This behaviour, may be the same as PVD at E_{Cu} = 30 eV for lower energies. The consequence of this is that a mixture of growth progresses will occur but most of which will dominated by layer-by-layer growth.

To accommodate the contribution of the system design, we now bring into play the contribution of E_{Cu} in IBAD. On 50% alternate bombardment and deposition cycles translates to one cycle for which 3D island formation is favoured and another cycle of layer by layer growth is favoured. This is because in the thermal energy zone ($\leq$ 1 eV) favours island formation (see Figure 11). This is in contrast to PVD whereby every simulation cycle (at 30 eV) favours formation of layer-by-layer growth. Therefore, part of the mishap witnessed in IBAD is due to the system (i.e. simulation setup) design. To try to correct the small misgiving in IBAD processes resulting from the 50% bombarding rate, an increase of energy in the system is attempted. This is a potential reason that supports the observed improvement of the layer-by-layer growth at 50 eV.

It has already been established in the literature that at energies 30 - 50 eV, a number of processes including layer-by-layer growth, sputtering, surface defects and expitaxy improvements can occur. This has been summarised in Figure 11 [22]. In addition, other studies have already deduced that at energies lower than 100 eV, Ar sputtering yield increases linearly with the square root of Energy [61]. This means that ion impingement at an energy of 50 eV has a higher likelihood of sputtering more atoms than 30 eV. Therefore, the management of island heights that form in the deposition cycle (at E_{Cu} = 1 eV) is achieved through sputtering. This process is more efficient for 50 eV under the assumption that no excessive ion milling is done unto the surface. This forms a potential basis of explanation to the difference in growth mode at E_{Ar} = 30 eV and at E_{Ar} = 50 eV.

In the event that no sputtering takes place, then, the amount energy transferred at 50 eV at any cycle is almost twice the amount at 30 eV. At 50% Ar fluence, the effect of bombardment delivered in one shot at E_{Ar} = 50 eV can be perceived to acts as a compensatory round for which no bombardment occurs. In other words, using E_{Ar} = 50 eV translates to an excess of $\sim$20 eV that is always available for additional atomic diffusion related activities in every bombardment cycle.

There is a critical size (radius) for which an island is stable. High energy collision that induces either sputtering or diffusion activities leads to destabilization of stable islands. An unstable island, is coerced by equilibrium forces either to disintegrate or acquire more atoms to restabilize. As alluded above that bombardment energy of 50 eV has greater influence on deposition process, then its influence in indirectly initiating equilibrium driven processes are also greater. This can also be partly attributed to the better layered profile at 50 eV.

3.2 Effect of Ar ion fluence on layer growth

It has been established that increasing Ar ion energy improves significantly layer-by-layer growth. The other simulation aspect that elicits curiosity is the effect of the ion-to-atom rate. It has been established that one of the potential causes of roughening in IBAD is the alternate bombarding cycle. What happens if the deposition frequency was lowered in IBAD process at high bombardment energy (30 eV)? Can this mimic a slow PVD at E_{Cu} =30 eV? To have some legitimate grounds of addressing these questions, a basic understanding of the effect of relative deposition rate on growth outcome will be illustrated below.

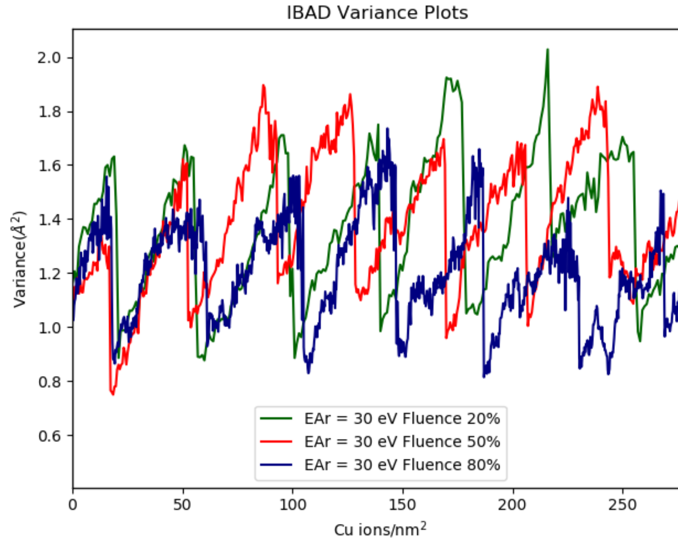

Figure 25: IBAD Ar ion Fluence modulated surface profile. The vertical scale has been magnified to spot the differences

Deposition done at an energy of E_{Ar} = 30 eV for different ion-to-atom rates show that a high ion-to-atom rate inhibits growth or formation of islands. In Figure 25, it can be seen that roughening is greatest for the lowest ion fluence. This can be seen in the rising variance profile of 20% fluence plot. The last part of that profile is a false decline in variance due to saturation artefacts. However, the profile at 80% fluence has a much better improvement to that of the initial 50% profile. This suggests that at lower deposition rate in comparison to the bombardment rate leads towards a better layer-by-layer profile.

The images in Figure 26 show that island formation is extremely quashed at 80% and the deposited film layers consist of highly ordered atomic layers. In the case of 20%, the farthest right edge is made up of incomplete atom stacks. This occurrence starts from the seventh layer (yellow atoms) to slightly below the sixth layer. The atomic ordering in these layers is visible but feeble in all top layers. This behaviour and of such magnitude is unique to 20% fluence. The interpretation of such extreme behaviour at 20% fluence is that island growth progresses faster than the layer-by-layer growth.

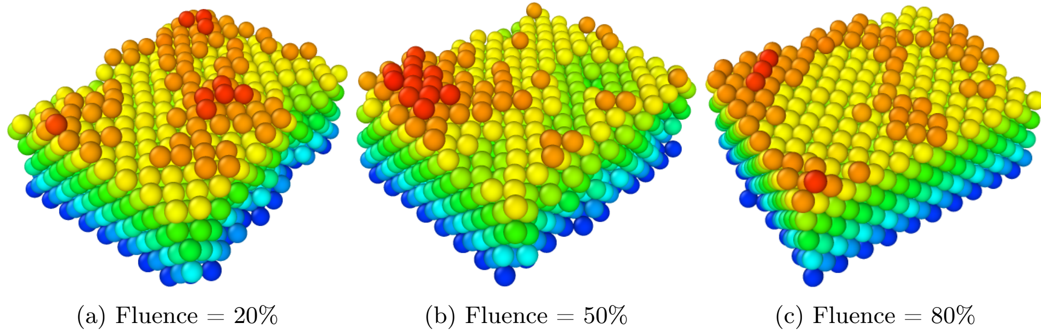
(a) Fluence = 20% (b) Fluence = 50% (c) Fluence = 80%

Figure 26: IBAD at E_{Ar} = 30 eV and Varied Fluence

Comparison between 0.5 ion/nm^2 and 0.8 ion/nm^2 fluence, shows that at at 0.8 ion/nm^2, the precision for which atomic ordering and film layer completion per monolayer is excellent. More so, it is free of defects assuming that islands of the 9th layer (red atoms) don't count. In summary, fluence of 0.2 ion/nm^2 is the roughest for which island growth supersedes layer-by-layer growth. In 0.5 ion/nm^2 fluence, layer-by-layer growth dominates but smooth growth is hampered by the presence of few islands. In the 0.8 ion/nm^2 case, highly ordered layer-by-layer growth is dominant with an extremely weak or zero interference by island growth.

There are two ways so far that have been seen to give good layer-by-layer deposition. One is to have a higher bombardment energy at 50 eV with fluence of 0.5 ion/nm^2, and the other would be to slow deposition and have low energy. A plot of quick comparison against the proclaimed standard PVD (E_{Cu} = 30 eV) looks as follows:

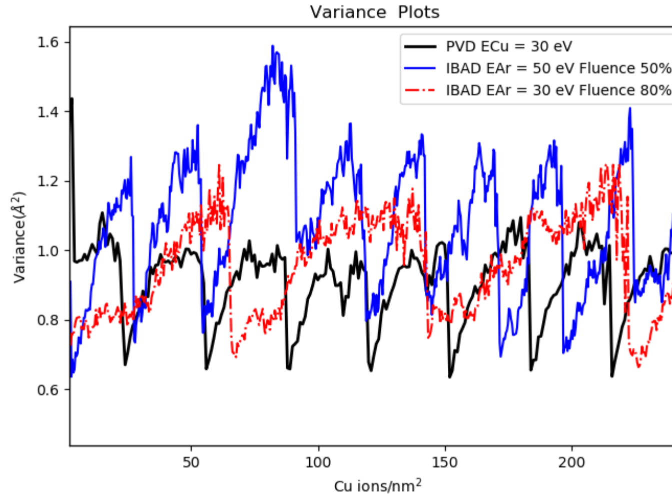

Figure 27: Comparison of the best layer-by-layer growth.

The variance plot shows that slow deposition at moderate bombardment energy produces closer or better layering in film as in the case of PVD at E_{Cu} = 30 eV. Therefore, it is most suitable to adopt a higher ion fluence (e.g. 0.8 ion/nm^2) in IBAD (E_{Cu} = 1 eV, E_{Ar} = 30 eV) for layer-by-layer film deposition. However, there is a catch to this approach. To grow 8 complete monolayers at 0.8 ion/nm^2 ion fluence takes approximately 6214 atoms. On the other hand, growing the same number of monolayers using fluence 0.5 ion/nm^2 IBAD (E_{Cu} = 1 eV, E_{Ar} = 50 eV) takes approximately 2900 atoms. This means that if fast growth rate is required in IBAD process, higher bombarding energies at a higher deposition rate would still give reasonable results. However, if speed were not of any importance, a high bombardment to deposition rate would be the most suitable deposition

process.

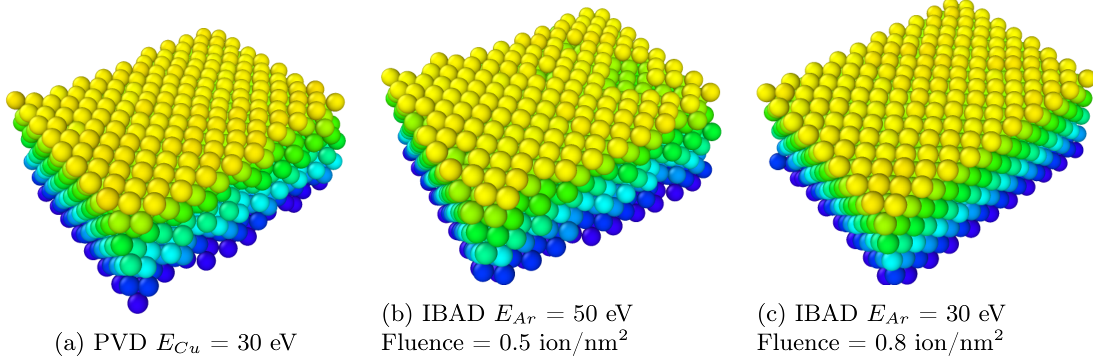

(a) PVD $E_{Cu} = 30$ eV (b) IBAD $E_{Ar} = 50$ eV Fluence $= 0.5$ ion/nm^2 (c) IBAD $E_{Ar} = 30$ eV Fluence $= 0.8$ ion/nm^2

Figure 28: Comparison bests IBAD profiles under variation of fluence and against reference PVD film

The images taken just at the onset of the eighth layer and exposing the $7th$ monolayer show similar surface coverage for PVD and 0.8 ion/nm^2 fluence bombardment. However, looking at the edges, IBAD (0.8 ion/nm^2) at its best delivers superior arrangement of atoms. The aspect ratio of IBAD is way superior than best PVD film growth. Therefore, for fast layer-by-layer deposition, PVD will do but for an excellent film where all details matter, IBAD done at a much lower deposition rate produces the best quality.

3.3 Film Stress

The stress profile follows closely to the Stoney's equation for which the stress takes a inverse association with distance/ thickness (along z). The vanishing stress state is due equal and opposite curvature of the film. The stress profile is locally discrete in nature probably representing the nature of the atomic positioning. The small distribution within the confined distances is rather a representation of slight anomalies in the atomic arrangement. This is a homoepitaxial growth, there is no stress contribution from lattice mismatch and we can assume that thermal effects do not contribute to the stress values since the film and substrate have same thermal expansion coefficients. More so, the contributions from vibrations will be ignored.

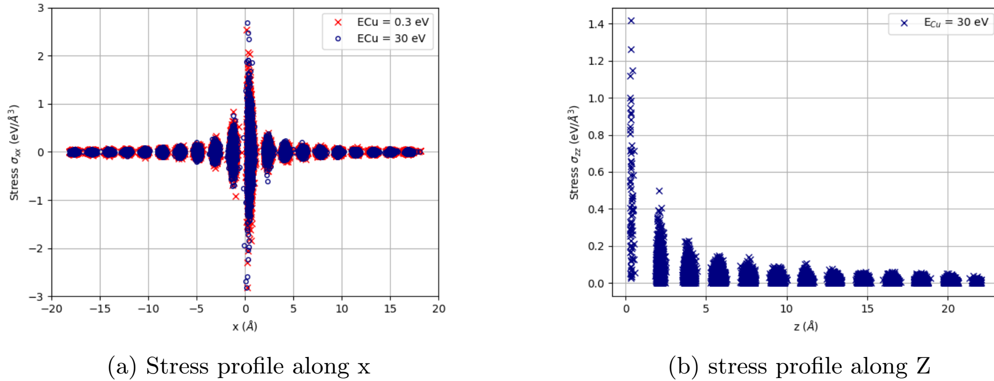

(a) Stress profile along x (b) stress profile along Z

Figure 29: PVD stress profiles

The initial surface is at equilibrium despite having a non-smooth surface. The addition of atoms in the initial substrate's surface causes disturbance in to this equilibrium. This is translated as stress.

In other words, the forces acting on the initial surface atoms are reorganised to accommodate the additional layer of atoms. This type of stress increases as elastic strain energy increases. However, the increase in stress reduces the total surface energy. This can be easily seen by considering Equation 3 that shows the effect of adding an atom on a surface, and Equation 4 that explains the increase of stress and strain energy. The decreasing stress with increasing thickness is due to local atomic rearrangement in that neighbouring island can coalesce or local diffusion processes that take place as deposition increases. However, the change is not zero as the absence of incomplete equilibrium process would still induce some stress.

The absolute stress profile on a scatter plot shows slightly distorted symmetrical profile along the stress axis ($\sigma_{xx} = 0$) as well the x-axis (x = 0). This is pronounced in the case of IBAD but heavily masked in PVD. However looking at the two plots around x = 0 shows some form of asymmetry. The distortion of stress symmetry with distance is a common phenomenon of thin films grown on rectangular substrates. The initial stresses can be attributed to film curvature for which an imbalance of compressive and tensile forces come into play. In the event that the film induces no curvature on the substrate, a large stress gradient forms. This stress gradient is relaxed by direct diffusion of atoms, growth or deformation of grain boundaries.

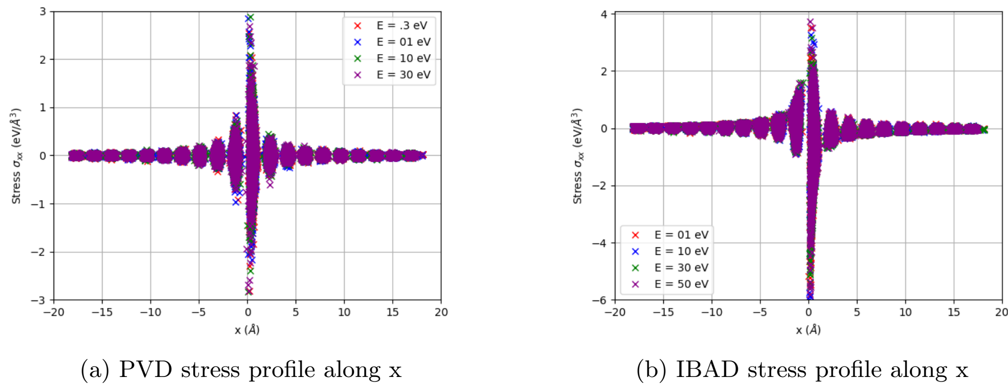

(a) PVD stress profile along x

(b) IBAD stress profile along x

Figure 30: stress profiles

The stress profile along z direction, direction of film thickness, are nearly identical for all deposition processes. There is clustering of stress points at certain areas within the plot.

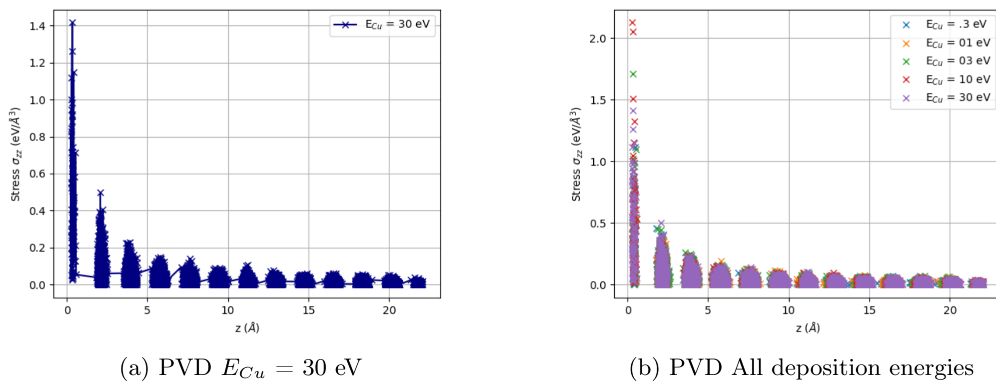

(a) PVD E_{Cu} = 30 eV

(b) PVD All deposition energies

Figure 31: PVD stress profiles

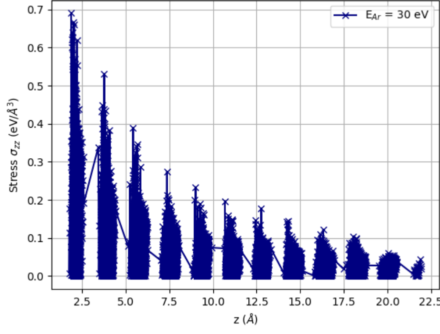

(a) IBAD $E_{Cu} = 1$ eV & $E_{Ar} = 30$ eV

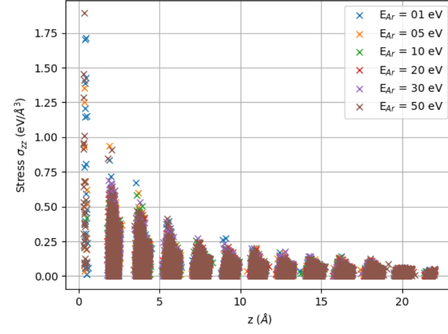

(b) IBAD All bombardment energies

Figure 32: IBAD stress profiles

The typical features are poorly represented by the huge number of points clustered within certain areas of thickness. Conventional methods of either smoothing or using signal envelop such as Hilbert transforms, Savit Golay filter and low pass Butterworth filter on their own do not produce any better means of discriminating profiles [62]. However, an implementation of OVITO like binning method produces much better profile when combined with filters. In binning, z step (dz) is calculated as $dz = (z_{max} - z_{min})/bins$ where z_{min} and z_{max} are the maximum and minimum values of z. The stress value is calculated on the basis of maximum value i.e. σ_{max} in the range $[z_i, z_{i+1})$. For example using 500 bins and Savit Golay filter (using a window of 31 points and polynomial of order 5) produces results shown in Figure 33a.

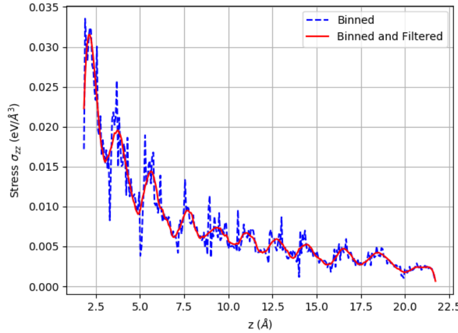

(a) Data binning and the resultant smoothed function using Savit-Golay filter

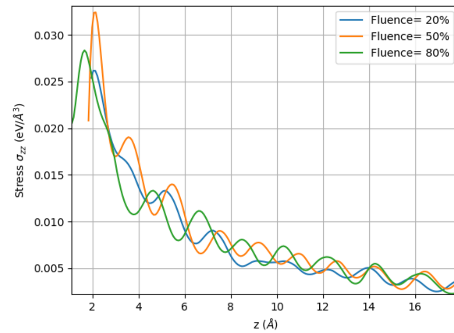

(b) IBAD ($E_Ar = 30$ eV) stress profile using binning and Savit-Golay filter

Figure 33: Binned and Smoothed stress profiles

The accuracy and quality of binning and filtering depends more on the number of bins used and the definition of the filter function. Low number of bins results in poor representation, while a large number of bins does not produce significantly different results from the original data points. Filtering leads to loss of details. In the event of very small differences in values (curves), the results is more catastrophic as shown in Figure 33b.

The stress profiles have minute differences. This means an attempt to over-process the data would result in the loss of minor deviations. Instead of using multiple processing methods, a single polynomial fit is used. In this case, a tenth order polynomial fit is applied uniformly across the profiles.

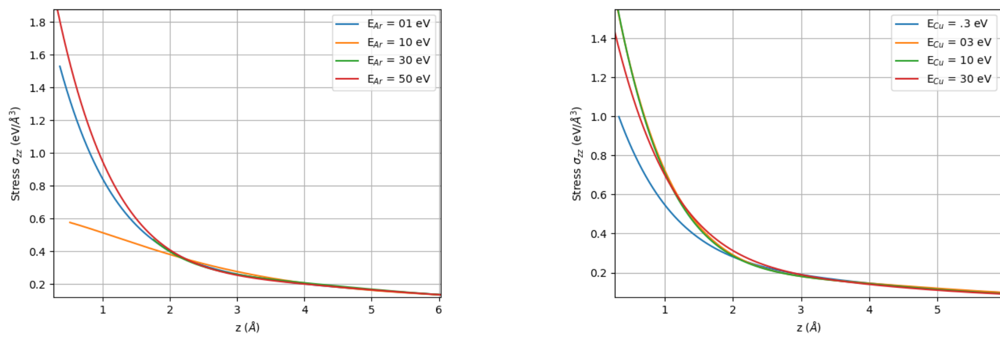

(a) IBAD (E_{Cu} = 1 eV & Fluence = 0.5) and varied bombardment energies

(b) PVD stress profile with different Cu deposition energies

Figure 34: Polynomial fitted stress profiles

As already mentioned, disturbance from equilibrium generates stress during deposition. Therefore, the converse will be true i.e. growth performed close to equilibrium conditions results in nearly stress free growth. In the kinetic perspective of atomic motion, a higher rate of atomic motion on the surface during deposition in comparison to the deposition rate favours film growth near equilibrium conditions. This is expected to result in minimal stressed structures. This is informed by understanding that an adatom is likely to find a suitable site on the surface which will least disturb surface equilibrium. The catch to this approach is that rapid kinetics (higher diffusion energies) are required [63].

In PVD, deposition at 0.3 eV, the film stress profile towards minimization limit is the slowest. The remaining profiles show almost the same traits for which the initial film is greatly stressed but finally stabilizes after thickness of 3 Å. In IBAD, ion bombardment at 10 and 30 eV show the least stressing of the film. At 30 eV, the stress profile is almost of comparable magnitude of the minimum stress level reached by all stress profile (constant minimum value). PVD reaches saturation fastest due to the 100% deposition cycle. The fast deposition rates means that non-equilibrium structure is always eminent. This, however, is not the only reason behind the film stress as in IBAD, at certain energies, the stress profiles also show noticeable level of stress.

The absolute stress magnitude in IBAD is less in comparison to that in PVD. This in some sense reflects slowed down deposition frequency in IBAD. On an equivalent energy basis, $E_{Ar} >$30 eV shows an increase in stress which would suggest that there is poor energy transfer mechanism or poor surface energetics responses. The implication of this observation is that at E_{Ar}=50 eV, the good surface profile that was previously observed has less to do with momentum transfer and perhaps more with the management of islands through sputtering.

Although this polynomial fit has provided a means of signal discrimination, it does not sufficiently give a consistent correlation of stress with either deposition or bombardment energy. In PVD, the least stressed profile is the one with the least mobility while in IBAD it is not the case. Despite all these, film grown under optimal PVD conditions is more stressed than IBAD. This can be deduced by the magnitude of stress at E_{Cu} = 30 eV (PVD) and E_{Ar} = 30 eV (IBAD).

Conclusion

PVD is a faster means of growing film on a substrate than IBAD. This has been seen in the time taken to attain the growth of a certain number of layers of interest. However, the quality of the film grown is not necessarily independent on the growth rate.

In pure PVD, low deposition energies are dominated by island growth while at intermediate to high energies layer-by-layer growth dominates. The quality of layering is, however, poorer at intermediate energies. It has been established that the highest quality epitaxial growth occurs at deposition energy of 30 eV

In IBAD, the layering quality increases primarily with ion bombardment energy. This is primarily due to the low deposition energy employed in this set up. This makes all surface migratory processes to be dependent on the Ar ion energy transfer. It is observed at an equal Cu deposition and Ar bombardment rates, the higher the energy, the better the layering. Very high bombardment energies diminishes the effectiveness of the deposition process. Sputtering of films and substrate becomes pronounced. At very low bombardment energies, the results are similar to PVD at low energies.

It is remarkable to note that at reasonable energies in the limit of perfect-layered PVD process, the Ar ion fluence determines the quality of the layer-by-layer film. At bombardment energies $\sim$ 30 eV, layer-by-layer deposition is predominant. However, at variation of fluence the final morphology vary from good to excellent film structure. It has been seen that at fluence of 0.5 the film quality layering is inferior to PVD grown film while at a fluence 0.8, the film quality is far superior to PVD grown film. The only costs of producing the ideal structure at 0.8 fluence is the deposition duration.

In addition, when IBAD is conducted in equal fluence of 0.5, much higher energy is required to produce similar surface morphology as PVD. This is the case at 30 eV against 50 eV bombardment energies. This has been attributed in the methodology of handling the deposition cycle. At bombardment energy of 50 eV, improved morphology is alluded to the compensatory mechanism in the cycle for which bombardment does not occur. The other reason is that at high energies, the means of island eradication is more efficient i.e. sputtering is much more efficient.

The overall stress reduces with the thickness of film up to a limiting value where by the stress takes an asymptotic value as a function thickness. The stress profile shows that in PVD at very low deposition energies, the film is least stressed in comparison with other deposition energy. In the case of IBAD, moderate to nearly minimum stress levels is observed with intermediate bombardment energies. However, the best growth profiles at 30 eV IBAD and PVD show that PVD is subjected to more stress during growth.

Finally, we note that the simulation is a good representation of the actual deposition process. However, the time scales for doing MD simulations are too fast compared to typical deposition rates. In principle this could be addresses by running surface kinetic Monte Carlo simulations between the MD deposition events, but linking the two methods is technically very demanding and beyond the scope of the current thesis.

References

[1] M-F. Lai et al.,Wafer-level three-dimensional integrated circuits (3D IC): Schemes and key technologies. Microelectronic Engineering (2011) 88:3282-3286.

[2] A. Mulay, Sustaining Moore's Law: Uncertainty Leading to a Certainty of IoT Revolution. (2015) Morgan & Claypool.

[3] S. M. Sze & M-K. Lee, Semiconductor Devices: Physics and Technology, 3rd Ed. (2012) John Wiley & Sons.

[4] M. Ohring, The Material Science of Thin Films. (2002) Academic Press.

[5] M. P. Allen & D. J. Tildesley, Computer Simulation of Liquids. (1991) Oxford Science.

[6] M. Turowski et al., Simulation in thin film technology. Proceedings of SPIE (2015) 9627:962707.

[7] C. Liu et al., Corrosion resistance of multi-layered plasma-assisted physical vapour deposition TiN and CrN coatings. Surface and Coatings Technology (2001)141:164-173.

[8] D. M. Mattox, Handbook of Physical Vapor Deposition (PVD) Processing. (1998) Elsevier.

[9] D. Hoffman et al. Handbook of Vacuum Science and Technology. (1997) Elsevier.

[10] Thin Film Consulting, Advancing Magnetron Sputtering Technology: Fundamentals of sputtering. $http://www.thfc.de/fundamentals-of-sputtering$

[11] J. D. Plummer, M. D. Deal& P. B. Griffin, Silicon VLSI technology fundamentals practice and modeling. (2000) Prentice Hall.

[12] S. J. Marrink et al., The MARTINI Force Field: Coarse Grained Model for Biomolecular Simulations. Journal Physical Chemistry B (2007) 111: 7812-7824

[13] B. P. Jurecka et al., Theoretical studies of RNA catalysis: hybrid QM/MM methods and their comparison with MD and QM. Methods (2009) 49:202-16.

[14] H. Lüth, Solid Surfaces, Interfaces and Thin Films. 5th Ed. (2015) Springer.

[15] H. Ibach, Physics of Surfaces and Interfaces. (2006) Springer.

[16] A. Mazor et al., Columnar growth in thin films. Physical Review Letters (1988) 60:1455

[17] J. A. Venables, Atomic processes in crystal growth. Surface Science (1994) 299–300:798-817

[18] C. V. Thompson, Structure Evolution During Processing of Polycrystalline Films. Annual Review of Materials Science (2000) 30:159-190

[19] Z. Crljen et al., Relaxation and Reconstruction on (111) Surfaces of Au, Pt, and Cu. Physical Review B (2003) 68:195411

[20] H-J. Butt, K. Graf & M. Kapp, Physics and Chemistry of Interfaces. (2003) John Wiley & Sons

[21] P. Wynblatt & N. A. Gjostein, A Calculation of Relaxation, Migration and Formation Energies for Surface Defects in Copper. Surface Science (1968) 12:109-127

[22] R. Eason, Pulsed Laser Deposition of Thin Films: Applications-Led Growth of Functional Materials. (2006) John Wiley & Sons.

[23] K. Oura et al., Surface Science: An Introduction. (2010) Springer.

[24] J. Dorsch, Semiconductor Manufacturing and design community: New Applied PVD system targets TiN hardmasks for 10nm, 7nm chips.(2015) *http://semimd.com/blog/tag/pvd/*

[25] S. C. Lyu et al., Low-Temperature Growth of ZnO Nanowire Array by a Simple Physical Vapor-Deposition Method. Chemistry of Materials (2003) 15:3294-3299

[26] R. A Laudise, et al., Physical vapor growth of organic semiconductors. Journal of Crystal Growth (1998) 187:449-454

[27] B. L. Houseman, B. E. Marzocchi & G. C. Towson, The Influence of Substrate Temperature on the Sticking Coefficient of Zinc on Glass. Defense Technical Information Center (1968)

[28] S. Abela, Physical vapour deposition of magnesium alloys, Surface Engineering of Light Alloys, (2010) Chapter 9:294-322. Woodhead

[29] H. Nomura, et al., Ion Beam Processing and Analysis of MgO Thin Films.(2003) American institute of physics 680. DOI: 10.1063/1.1619791.

[30] H. Shang, J. Li & T. Shao, Mechanical Properties and Thermal Stability of TiN/Ta Multilayer Film Deposited by Ion Beam Assisted Deposition. Advances in Materials Science and Engineering(2014) 2014:1-8

[31] H. Brune, Growth Modes. Encyclopedia of Materials: Science and Technology, Sect. 1.9, Physical Properties of Thin Films and Artificial Multilayers, 3683-3693.

[32] M. Ritala, Thin Film lecture material. Section 11: Nucleation and evolution of film structure *https://courses.helsinki.fi/fi/matr361/119745336*

[33] M.S. Daw et al., The embedded-atom method: a review of theory and applications. Materials Science Reports (1992) 9: 251-310.

[34] Y. H. Chui et al., Modeling the crystallization of gold nanoclusters—the effect of the potential energy function. Journal of Physics: Condensed Matter (2009) 21:144207.

[35] A. Kuronen, Molecular dynamics simulation of atom-atom collisional scattering. Journal of Physics: Condensed Matter (1991) 3:1363-1370.

[36] Sandia Corporation, LAMMPS Documentation.
https://LAMMPS.sandia.gov/doc/pair_zbl.html

[37] J. Kang, Y. Hagiwara & M. Tateno, Biological applications of hybrid quantum mechanics/molecular mechanics calculation. Journal of biomedicine & biotechnology (2012) 2012: 236157.

[38] Oleg M. Braun, Computer Modeling in Physics, Institute of Physics National Academy of Sciences of Ukraine

[39] A. Torre,Linear Ray and Wave Optics in Phase Space: Bridging Ray and Wave Optics via the Wigner Phase-Space Picture. (2005) Elsevier.

[40] M.J. Abraham & the GROMACS development team, GROMACS User Manual version 2019.1: Chapter Five *http://www.gromacs.org*

[41] M. O. Steinhauser, Introduction to Molecular Dynamics Simulations: Applications in Hard and Soft Condensed Matter Physics, 2012.

[42] V.A. Luchnikov, M.L. Gavrilov, N.N. Medvedev & V.P. Voloshin, The Voronoi–Delaunay approach for the free volume analysis of a packing of balls in a cylindrical container. Future Generation Computer Systems (2002) 18:673 - 679.

[43] J. Janecek, Influence of the Periodic Boundary Conditions on the Fluid Structure and on the Thermodynamic Properties Computed from the Molecular Simulations. Oil & Gas Science and Technology (2013), 68:187-396.

[44] L. R. Pratt & S. W. Haan, Effects of periodic boundary conditions on equilibrium properties of computer simulated fluids. I. Theory. Journal of Chemical Physics (1981) 74:1864.

[45] Monticelli et al.,The MARTINI Coarse-Grained Force Field: Extension to Proteins. Journal of Chemical Theory and Computation (2008) 4:819–834.

[46] Murtola T1, Falck E, Karttunen M, Vattulainen I. Coarse-grained model for phospholipid/cholesterol bilayer employing inverse Monte Carlo with thermodynamic constraints. Journal of Chemical Physics (2007) 126:075101.

[47] Y-C. Chien et al., Modulation of Calcium Oxalate Dihydrate Growth by Selective Crystal-face Binding of Phosphorylated Osteopontin and Polyaspartate Peptide Showing Occlusion by Sectoral (Compositional) Zoning, Journal of Biological Chemistry (2009) 284:23491–23501.

[48] S. M. Foiles, M. I. Baskes & M. S. Daw, Embedded-Atom-Method Functions for the fcc Metals Copper, Silver, Gold, Nickel, Palladium, Platinum, and Their Alloys. Physics Review. B, Condensed Matter (1986) 33:7983-7991.

[49] M. S. Daw, S. M. Foiles & M. I. Baskes, The embedded-atom method: a review of theory and applications. Materials Science Reports (1993) 9:251-310.

[50] R. Delgado-Buscalioni, J. Sablić & M. Praprotnik, Open boundary molecular dynamics. The European Physical Journal Special Topics (2015) 224:2331-2349

[51] Y. S. Lavrinenko, I. V. Morozov & I. A. Valuev, Reflecting boundary conditions for classical molecular dynamics simulations of nonideal plasmas. Journal of Physics: Conference Series (2016) 774:012148.

[52] P. H. Hünenberger, Thermostat Algorithms for Molecular Dynamics Simulation. Advances in Polymer Science (2005) 173:105–149.

[53] A. Djaafri et al., Computer Simulation Studies of Collision Cascade in Tantalum. The African Review of Physics (2013) 8:0051

[54] N. Schwarzer & F. Richter, On the determination of film stress from substrate bending: Stoney's formula and its limits.
$https://monarch.qucosa.de/api/qucosa\%3A18453/attachment/ATT-0/$

[55] A. Stukowski, OVITO User Manual (2017) $https://www.ovito.org/manual/$

[56] B. Bhushan, Modern Tribology Handbook, Two Volume Set. Chapter 2: Surface Roughness Analysis and Measurement Techniques (2001) Boca Raton: CRC Press.
$https://doi.org/10.1201/9780849377877$

[57] F. L. Forgerini & R. Marchiori, A brief review of mathematical models of thin film growth and surfaces. A possible route to avoid defects in stents. Biomatter (2014) 4:e28871

[58] S. Xu et al., Properties of carbon ion deposited tetrahedral amorphous carbon films as a function of ion energy. Journal of Applied Physics (1996) 79:7234

[59] L. M. Dupuy and R. E. Rudd, Surface identification, meshing and analysis during large molecular dynamics simulations. Modelling and Simulation in Materials Science and Engineering (2006) 14:229–251

[60] A. P. Thompson, S. J. Plimpton & W. Mattson, General formulation of pressure and stress tensor for arbitrary many-body interaction potentials under periodic boundary conditions. Journal of Chemical Physics (2009) 131:154107

[61] F. Greer et al., Argon and oxygen ion chemistry effects in photoresist etching. Journal of vacuum science & technology B (2002) 20:1901-1905

[62] The Scipy community, Signal processing.
$https://docs.scipy.org/doc/scipy-0.16.1/reference/signal.html$

[63] F. Doerner & W. D. Nix (1988) Stresses and deformation processes in thin films on substrates. Critical Reviews in Solid State and Material Sciences (1988) 14:225-268